

**DETECTION OF CIRCULATING BREAST CANCER
CELLS USING PHOTOACOUSTIC FLOW CYTOMETRY**

A Thesis presented to
the Faculty of the Graduate School
at the University of Missouri

In Partial Fulfillment
of the Requirements for the Degree
Master of Science

by
KIRAN BHATTACHARYYA
Dr. John Viator, Thesis Supervisor
MAY 2013

The undersigned, appointed by the Dean of the Graduate School, have examined the thesis entitled:

DETECTION OF CIRCULATING BREAST CANCER CELLS
USING PHOTOACOUSTIC FLOW CYTOMETRY

presented by Kiran Bhattacharyya,

a candidate for the degree of Master of Science

and hereby certify that, in their opinion, it is worthy of acceptance.

Dr. John Viator, Biological Engineering

Dr. Gang Yao, Biological Engineering

Dr. Mark Hannink, Biochemistry

ACKNOWLEDGMENTS

In completing this thesis, I would like to acknowledge Dr. Viator for all of his help and mentoring through the 7 years that I've been here. He provided the opportunities and training which has made me the scientist I am today. Since it will make this thesis many pages longer if I continue to elaborate on Dr. Viator's support through the years, I will leave it by saying that I am forever in his debt for this and much more. I cannot go on without also thanking Dr. Hannink and Dr. Yao for being on my committee and providing me with much needed guidance.

I would also like to thank the members of the VIATOR Lab who have helped me countless number of times, especially Ben Goldschmidt, Devin McCormack and Christine O'Brien. Not only were they work colleagues but they were also my close friends with whom I could vent research frustrations and celebrate research victories, which sometimes seemed to be far and few between.

I would also like to thank Dr. Borgelt, who may not have helped with the writing of this thesis, but gave me the opportunity to round out my graduate education by allowing me to teach classes. It helped me understand more clearly the connection between the lab and the classroom.

I would like to thank my students who were patient with me as I walked the learning curve of mentorship. Though it is a cliché, it's true that they often taught me more than I taught them.

I would like to thank my parents, Kakoli and Sanjib Bhattacharyya, without whom there would be nothing. They planted the germ of my ambition when I was young and have nourished it by being a source of everlasting encouragement. I have to acknowledge my big brother, Surya Bhattacharyya, who has always been there for me as a friend and an extra parent.

Finally, I would like to acknowledge my girlfriend, Rachel Fischer, who kept me in great spirits and has tolerated my obsession with science especially regarding the long hours and arduous work needed to complete this thesis. I am grateful for her company, her moral support, and her efforts to help me reach my own goals.

There are undoubtedly others who have contributed or helped me in some way and have not been mentioned. I would like to thank everyone who has helped me come this far and those with whom I'll embark on the next leg of my journey.

TABLE OF CONTENTS

ACKNOWLEDGMENTS	ii
LIST OF TABLES	vi
LIST OF FIGURES	vii
ABSTRACT	ix
Chapter	
1 INTRODUCTION	1
1.1 Breast Cancer	1
1.2 Metastatic Cancer	4
1.2.1 General Metastasis	4
1.2.2 Breast Cancer Metastasis	7
1.3 The Photoacoustic Effect	8
1.4 Biomedical Photoacoustics	11
1.5 Gold Nanoparticles	13
1.5.1 Gold Nanoparticles in Photoacoustics	14
1.6 Flow Cytometry	15
1.7 Photoacoustic Flow Cytometry	16
2 NANOPARTICLE CONJUGATION AND DETECTION OF BREAST CANCER CELLS	20
2.1 Nanoparticle Analysis and Antibody to Nanoparticle Conjugation	20
2.1.1 Optical Properties of the Nanoparticles	20
2.1.2 Conjugation Protocol	24
2.2 Nanoparticle Attachment to Cancer Cells	25
2.3 Black Microspheres as Cancer Cell Phantoms	28
2.3.1 Microsphere Tests	29
2.3.2 Global Analysis of Entire Flow Chamber	30
2.3.3 Microsphere Signal Analysis	31
2.3.4 Re-Analysis of Entire Flow Chamber	33

2.4	Breast Cancer Cell Tests	36
2.4.1	Breast Cancer Cell Signal Analysis	37
2.4.2	Breast Cancer Cell Detection Limit	39
3	BREAST CANCER CELL DETECTION IN SALINE AND FROM NORMAL BLOOD	41
3.1	PAFC Detection	41
3.2	Nanoparticle Attachment to Breast Cancer Cells	42
3.3	Cell Preparation	42
3.4	Classification in Saline	43
3.5	Detection from Normal Blood	46
3.5.1	Blood Centrifugation Procedure	46
3.5.2	Results from the Blood Test	49
3.5.3	Captured Cancer Cells	50
3.5.4	Discussion of Results	50
4	THE ISSUE OF NON-SPECIFIC LABELING	54
4.1	EpCAM as the Target	54
4.2	Non-specific Interactions Without Antibodies	55
4.2.1	Non-specific Interaction of Fluorescent Spheres	56
4.2.2	Non-specific Interaction of Gold Particles	56
4.3	Binding of Fluorescent-Gold anti-EpCAM Conjugate to Cells	57
4.4	Implications of Non-specific Labeling	59
4.5	Further Research on Target Antigens	61
5	SUMMARY AND CONCLUDING REMARKS	63
APPENDIX		
A	Calculations for Antibody-Nanoparticle Conjugation	65
A.1	AuNPs to Anti-EpCAM on Fluorescent Bead	67
A.2	Nanoparticle Conjugate Storage	68
BIBLIOGRAPHY		
VITA		
		78

LIST OF TABLES

Table		Page
2.1	Expected Value of 2 Events	29
2.2	Expected Value of 4 Events	29

LIST OF FIGURES

Figure	Page
1.1 Breast Cancer Mammogram	3
1.2 Exponential Decay of Light in Absorbing Media	9
1.3 Photoacoustic Plane Wave	10
1.4 Absorption Spectra of Hemoglobin and Melanin	12
1.5 Gold Nanoparticle Size and Optical Absorption	14
1.6 Traditional Flow Cytometer	15
1.7 Photoacoustic Flow Cytometry	18
2.1 Set-up For Photoacoustic Absorption Spectrum	22
2.2 Absorption Spectra of Gold Nanoparticles	23
2.3 SEM Images of Dual-Modality Nanoparticles	25
2.4 Nanoparticle Tagged and Un-tagged Cells	26
2.5 Nanoparticle Tagged Cell: 3D Reconstruction	27
2.6 Black Microsphere PA Signal and Spectrum	32
2.7 Black Microsphere: Frequency Dependent Energy Content	33
2.8 Threshold Classification of Microsphere Signals	35
2.9 Breast Cancer Cell PA Signal and Spectrum	37
2.10 Breast Cancer Cell: Frequency Dependent Energy Content	38
2.11 Threshold Classification of Breast Cancer Cell Signals	39
3.1 Breast Cancer Signals from PAFC Test	43
3.2 Feature Space Plot of Breast Cancer Cells in Saline	44
3.3 Breast Cancer Signals from Blood Test	47
3.4 Feature from Blood Test	48
3.5 PAFC Captured Breast Cancer Cells	48
3.6 Cell Capture Using Micromanipulator	50

3.7	Cell Capture in Micro-well Array	53
4.1	Nanoparticle Labeling of Leukocyte	58
A.1	Fluorescent-AuNP Schematic	66

DETECTION OF CIRCULATING BREAST CANCER CELLS USING PHOTOACOUSTIC FLOW CYTOMETRY

Kiran D. Bhattacharyya

Dr. John A. Viator, Thesis Supervisor

ABSTRACT

According to the American Cancer Society, more than 200,000 new cases of breast cancer are expected to be diagnosed this year. Moreover, about 40,000 women died from breast cancer last year alone. As breast cancer progresses in an individual, it can transform from a localized state to a metastatic one with multiple tumors distributed through the body, not necessarily contained within the breast. Metastasis is the spread of cancer through the body by circulating tumor cells (CTCs) which can be found in the blood and lymph of the diagnosed patient. Diagnosis of a metastatic state by the discovery of a secondary tumor can often come too late and hence, significantly reduce the patient's chance of survival. There is a current need for a CTC detection method which would diagnose metastasis before the secondary tumor occurs or reaches a size resolvable by current imaging systems. Since earlier detection would improve prognosis, this study proposes a method of labeling of breast cancer cells for detection with a photoacoustic flow cytometry system as a model for CTC detection in human blood. Gold nanoparticles and fluorescent polystyrene nanoparticles are proposed as contrast agents for T47D, the breast cancer cell line of choice. The labeling, photoacoustic detection limit, and sensitivity are first characterized and then applied to a study to show detection from human blood.

Chapter 1

Introduction

1.1 Breast Cancer

Cancer is a type of disease in which human cells mutate and grow uncontrollably, no longer functioning correctly as a part of the biological system. Cancer is thought to be initiated by the carcinogenesis (mutagenesis) of pre-mitotic, determined but undifferentiated stem cells. A malignant tumor is a localized collection of cancer cells which are characterized by increased tissue density and vascular profusion. Most types of cancer have the ability to become metastatic by developing secondary tumors in organs distant from the locale of the primary tumor.

Breast cancer starts in the breast tissue which is composed of lobules and ducts surrounded by connective and fatty tissue. Some breast cancers are *in situ*, meaning tumors are still contained within the ducts and lobules. However, most breast cancers are invasive, starting in lobules and ducts but eventually breaking through the ductal and glandular walls into the adjacent tissue (ACS, 2013). Though breast exams or imaging results can strongly suggest the presence of breast cancer, a microscopic analysis of a tissue sample collected through surgical or needle biopsy is necessary for clinical diagnosis (ACS, 2013). Any cancer detection method, to reach clinical viability, must allow for this microscopic analysis or biochemical and immunochemical investigations.

The disease state of the patient is determined at the first diagnosis and continually updated to track the performance of treatment techniques. There are currently two

methods of staging cancer, the TNM classification system and the SEERS method. The TNM method uses the tumor size and proliferation to regions near the breast (T), lymph node biopsy (N), and distant metastases (M) to decide the disease state of the patient within a range of 0, I, II, III, or IV (ACS, 2013). Stage 0 being *in situ* and stage IV being the most advanced cancer, proliferated to the farthest regions of the body. On the other hand, the Surveillance, Epidemiology, End Results Summary (SEERS) staging system is largely used by cancer registries and public health research and planning. Local, Regional, and Distant stages are used to classify cancer patients in the SEERS method with class headings modifying tumor distribution in the patient's body.

Research evidence has shown that certain breast cancer subtypes have been associated with more favorable prognosis. Breast cancers which are estrogen receptor (ER) and/or progesterone receptor (PR) positive are generally more responsive to hormonal therapies while those that lack those receptors are associated with less favorable prognosis (ACS, 2013). However, currently receptor specific treatments are being developed that are improving the survival rates of the different subtypes of breast cancer patients.

Incidence of breast cancer in genetically related family members significantly increases the chances of an individual to be afflicted with breast cancer. Though other risk factors have also been identified, there is no certain way to prevent breast cancer, making early detection the only dependable strategy. Current detection guidelines for women vary by age but include mammography, clinical breast examination, and magnetic resonance imaging (MRI) for women at high risk. The American Cancer Society recommends that women with a greater than 20% chance of developing cancer at some point in their life should be annually screened with both MRI and mammography (ACS, 2013).

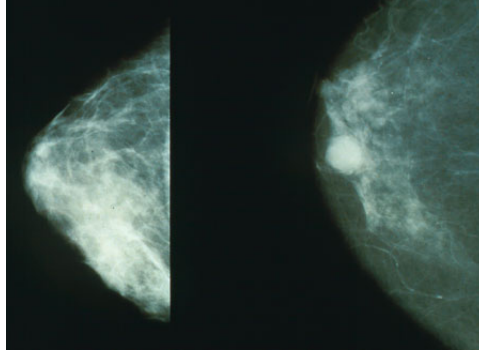


Figure 1.1: An image taken from a mammogram showing a normal breast to the left and a breast with cancerous growth to the right. White areas denote tissue with higher density and the cancerous growth on the right breast is a localized region of higher density tissue. It can be inferred from this figure that it is difficult to diagnose the presence of a cancerous tumor just from a mammogram due to the general similarity of both images. Image was retrieved from <http://en.wikipedia.org/wiki/File:Mammobreastcancer.jpg>

Current methods in clinical practice using MRI or CT imaging techniques can non-invasively find tumors embedded in human tissue. Although, these imaging methods can simultaneously scan large portions of the body for tumors, they lack the ability to resolve tumors under a few millimeters in size (Furman-Haran *et al.*, 2001). Though mammography is recommended by most doctors for patients with high risk of breast cancer, it is prone to false positives and negatives as evident in Figure 1.1, bringing into question the specificity of detection (Huynh *et al.*, 1998). Minor-invasive techniques include lymph node biopsies, which have higher sensitivity (tumor size $<1\text{mm}$) but often produce false negatives because the cancer either never interacted with the specific lymph node that is excised or the lymphatic system entirely (ACS, 2013).

1.2 Metastatic Cancer

1.2.1 General Metastasis

Cancer is generally not a localized disease. This is due to the ability of malignant cells to spread throughout the body of the host creating secondary tumor growths in distant areas. This can happen even before the primary tumor is discovered. The process of the spread of cancer is called metastasis. Tumors are not homogenous but rather are a collection of diverse cell types of the same kind of cancer (Gupta & Massague, 2006; Weigelt *et al.*, 2005). Only a minority of these various types of cells are capable of metastasis and surviving the cascade of events necessary to generate secondary tumors (Gupta & Massague, 2006; Dick, 2003; Fillmore & Kuperwasser, 2008). McKinnel *et al.* (2006) list the following as the interrelated events necessary for metastasis:

- (1) Disruption of Basement Membrane (required for all epithelial cancers)
- (2) Cell Detachment
- (3) Cell Motility
- (4) Invasion
- (5) Penetration of Vascular System
- (6) Circulating Cancer Cells
- (7) Arrest (stasis)
- (8) Extravasation and Proliferation

Since most malignancies are epithelial carcinomas, metastatic cells must be able to degrade the adjacent basement membrane to gain access to the extra-cellular matrix which houses both lymphatic vessels and blood capillaries (McKinnel *et al.*, 2006). Multiple research groups have shown that carcinomas of varied types have specific

proteinases capable of catabolizing the components of the basement membrane, like collagen and fibronectin (Gupta & Massague, 2006; Weigelt *et al.*, 2005; McKinnel *et al.*, 2006).

Apart from the transgression of the basement membrane, the metastatic cells must also be capable of detaching from the primary tumor. After detachment these cancer cells invade and travel through the extra-cellular matrix, finally migrating across a vessel wall into a blood vessel. It is not yet known what initiates cancer cell locomotion and motility. However, atomic force microscopy studies determined that cells which compose the tumors of metastatic patients have a significantly more resilient cytoskeleton than normal cells, indicating that the cancer cells may be more capable of movement through tissue (Cross *et al.*, 2007).

It is thought that most epithelial cancer cells cannot survive the rapid circulatory transit system and are damaged or destroyed upon entrance into the blood vessel. Unlike blood cells which are capable of remaining viable after amazing distortions of shape caused by fluid pressure, the metastatic cancer cells are mutated epithelial cells which never evolved to enter the circulatory system and are incapable of living through such changes, even with the extra resiliency of the cytoskeleton. However, a few minorities of cells do survive and express the metastatic potential (McKinnel *et al.*, 2006).

Extravasation, or leaving the circulatory system, and motility of the cell is again required to establish the secondary tumor which will now largely be composed only of the metastatic cancer cell type. For this reason, metastasis of metastases is an almost inevitable event. Therefore, the prognosis of metastatic cancer patient is much worse than that of the non-metastatic counterpart (Gupta & Massague, 2006; Weigelt *et al.*, 2005).

Detection and characterization of these circulating tumor cells which spread can-

cer is considered a clinically important goal. Monitoring the concentration of these metastatic cells in the blood of patients over time could prove to be an effective method of quantifying the disease state of the patient (Paterlini-Berchot & Benali, 2007). These measurements could become a staple in the process of staging cancer using the TNM method. Furthermore, molecular analysis of circulating tumor cells could shed much needed light on the process of metastasis (Sloan & Anderson, 2002; Hinton *et al.*, 2010). For instance, the knowledge of the cell surface markers and proteins which modulate or direct cell motility and invasion into vascularity could provide for new methods of cancer therapy.

Since this movement of metastatic cancer cells into vascularity can be likened to reverse leukocyte migration (from inflamed or infected tissue into lymphatic or blood vessels), similar mechanisms and proteins may play a role. Additionally, exogenous chemo-attractive or chemo-repulsive agents may steer the metastatic cell during its journey through the extracellular matrix by controlling extra- and intracellular signaling mechanisms (Hazan *et al.*, 2000). Studies on migrating neurons have shown high actin remodeling and cytoskeleton restructuring rates within the cell during movement; similar processes could be active during cancer metastatic motility. Identification of exogenous and endogenous proteins involved in the cascade from microenvironment sensing to actin remodeling for the sake of cellular locomotion could provide for direct methods of literally halting the spread of cancer (Hazan *et al.*, 2000).

Metastasis is a complicated event likely controlled by a multiplicity of genetic and epigenetic factors. Recently, there has been a growing interest in identifying genes that induce or suppress metastasis in order to elucidate the molecular mechanisms associated with the spread of cancer. About two-thirds of cancer patients have cancer which has already metastasized at the time of diagnosis (ACS, 2013). Since metastasis

accounts for 90% of deaths from solid tumors, it is important to reduce that proportion through early detection and understand the process so that it may be stopped.

1.2.2 Breast Cancer Metastasis

Breast cancer generally metastasizes to the bone, lung, liver, or brain (Weigelt *et al.*, 2005). It is thought that the primary tumor is a heterogeneous population of cells which evolve over time and that certain cells can develop the signaling molecules appropriate for the microenvironment of metastasis, e.g. bone, brain, etc. (Gupta & Massague, 2006). Circulatory patterns are not enough to dictate where a tumor cell within vascularity will deposit. There are preferred sites for metastasis as first shown epidemiologically by Paget in his seed and soil theory (Gupta & Massague, 2006; Weigelt *et al.*, 2005).

Since different functions and proteins are necessary to colonize biologically disparate environments, metastasis is an inherent and intrinsic feature of breast cancer cells. Therefore, the metastatic potential may be inferred at early stages in the primary tumor. It is expected that only a portion of the cancer cells harbor a tumor initiating capacity – the breast cancer stem cells (Dick, 2003; Fillmore & Kuperwasser, 2008).

Development of DNA microarray analysis in the recent past coupled with RT-PCR amplification has allowed the scientific community to study the gene expression signatures of single or groups of cells with great accuracy. DNA microarray, a transcriptional detector, can help identify patterns of gene expression to help classify heterogeneous groups of cancer cells into categories with supervised and unsupervised machine learning algorithms. This classification method could help identify genes which are overexpressed in primary tumors with greater propensity of metastasize. For instance, Ramaswamy *et al.* (2002) provide a list of 17 gene signatures associated

with metastasis in different cancers. Moreover, van de Vijver *et al.* (2002) developed a 70 gene classifier which had an 89.5% accuracy rate in classifying patients into a metastatic or non-metastatic group.

Furthermore, these markers could also give an indication of the environment of likely metastasis. For example, certain gene signatures of breast cancer tumor cells have been identified which correlate more with metastasis to bone than any other environment (Sloan & Anderson, 2002). Additionally, the role of the expression of CXCR4 and CXCL12, which have been correlated to increased metastasis in breast cancer, has been studied in brain metastasis (Hinton *et al.*, 2010). Circulating tumor cells captured with the photoacoustic flow cytometer could be tested with DNA microarray analysis for these gene sequences in order to determine the likelihood and locale of metastasis.

1.3 The Photoacoustic Effect

The photoacoustic effect is a physical phenomenon simply described as the transformation of light energy into acoustic energy. Incident light energy absorbed by a sample induces heating and expansion which creates a pressure gradient within the sample as seen in Figure 1.2. Localizing the irradiation both spatially and temporally, therefore localizing the pressure, generates an acoustic wave (Rosencwaig & Gersho, 1976). This acoustic wave can be analyzed to determine optical properties of the sample (Dumitras *et al.*, 2007).

In the past, due to the absence of monochromatic and pulsed light sources (Q-switched or mode-locked lasers), the photoacoustic effect was studied using chopped white light or CW lasers (Wong *et al.*, 1978; Suemune *et al.*, 1985; Rooth *et al.*, 1990). However, high power nanosecond or femtosecond laser pulses can provide

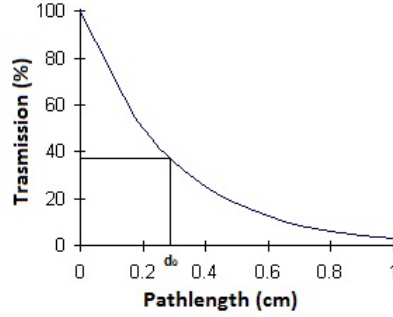


Figure 1.2: This plot shows the exponential decay of light in an absorbing medium as a function of the path length. The characteristic optical penetration depth is labelled as d_0 where about 36.7% of the light intensity is transmitted while the rest has been absorbed.

more accurate information about the optical characteristics of the irradiated sample. This conclusion can be reached by investigating the equation currently thought to define the pressure gradient of the planar acoustic wave generated in a homogeneously absorbing sample by the photoacoustic effect due to an ultra short laser pulse (Paltauf & Schmidt-Kloiber, 1997)

$$p(z, t) = \frac{1}{2}\mu_a\Gamma H_0(e^{-\mu_a(z-ct)} + e^{-\mu_a(z+ct)}) \quad (1.1)$$

In Equation 1.1, μ_a is the absorption coefficient, Γ is the Gruneisen parameter, e is the natural number, and z is the optical path length. The photoacoustic signal generated from a sample is directly related to the optical absorption coefficient of the sample at the wavelength of irradiation. Given that certain parameters are met, the photoacoustic wave mirrors the exponential absorption profile of the light intensity within the absorbing medium. Knowing the pressure gradient and the radiant exposure of the irradiation, the optical absorption of the sample can be calculated.

In Figure 1.3, the image depicts a situation in which an optical fiber irradiates an absorbing solution of red dye with pulsed light. Though not noted, the diameter of

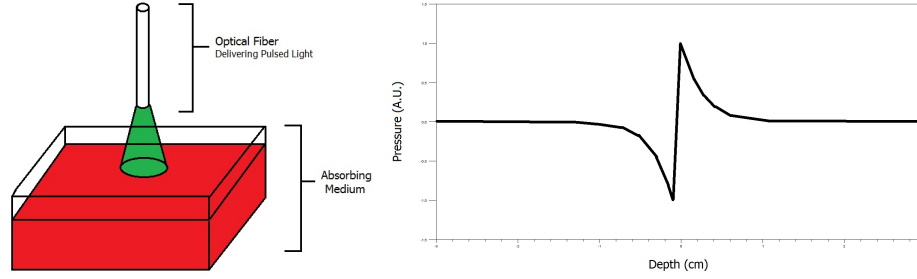


Figure 1.3: In the picture(left), an optical fiber delivers pulsed light and irradiates a region of the of an absorbing solution, here a red dyed liquid. The plot(right) shows the possible photoacoustic wave emitted by the sample.

the beam spot must be much larger than the optical penetration depth in the medium to excite a plane wave. The excited photoacoustic wave would resemble the plot on the right where the positive pressure gradient travels into the liquid and the negative portion is an acoustic reflection at the solution-air interface. Both pressure gradients are directly proportional to the absorption profile of light in the medium (Figure 1.2).

However, the plane wave equation is based on the assumption that all of the light energy is deposited instantaneously into the sample. Without this stipulation, the pressure gradient created is more difficult to analyze mathematically. The necessity of instantaneous energy deposition is an indirect effect of the need for stress confinement. Since the acoustic wave starts travelling as soon as stress is generated due to optical heating (during the laser pulse), the irradiating laser pulse must be much shorter than the time required for an acoustic wave to travel the characteristic optical penetration depth in the material.

$$\tau < \delta/c \tag{1.2}$$

Where τ is the duration of the laser pulse which is exciting the photoacoustic effect, δ is the characteristic optical penetration depth in the absorber, and c is the speed of sound in the medium. This inequality will ensure the approximate equivalent

of an instantaneous optical energy deposition. Due to the restriction on laser pulse duration, mode-locked or Q-switched lasers are choice candidates for scientific photoacoustics since the pulse duration is on the femtosecond-nanosecond scale, within which time length sound cannot travel any appreciable distance.

1.4 Biomedical Photoacoustics

Photoacoustics has widespread applicability as an imaging and sensing modality due to its specificity, as determined by the optical characteristics of the material, and ease of detection, as the generated acoustic signal is often robust and in the presence of no other acoustic sources. However, photoacoustics in the optical regime requires the sample being investigated to be pigmented.

Photoacoustic imaging can easily exploit the absorption of blood in the visible and NIR region of the light spectrum in order to detect and image *in vivo* vascularity. Zhang *et al.* (2009a) were able to image superficial vascular anatomy due to distinct optical absorption differences between blood and surrounding tissue. Additionally, Maslov *et al.* (2008) have shown the power of this technique by creating photoacoustic microscopy, a new imaging modality which marries optical contrast with ultrasound detection. Photoacoustics has also been successfully applied by Viator *et al.* (2002) to image and find depth profiles of port wine stains, caused by dilated venules in the reticular dermis. Sethuraman *et al.* (2008) even developed an intravascular imaging method for arteriosclerosis.

Melanin, the other major pigment in the body apart from hemoglobin, is also a common target for photoacoustic detection and imaging. Viator *et al.* (2004) were able to determine epidermal melanin content with photoacoustic methods while Zhang *et al.* (2006) imaged a melanoma tumor *in vivo*. Additionally, there has been

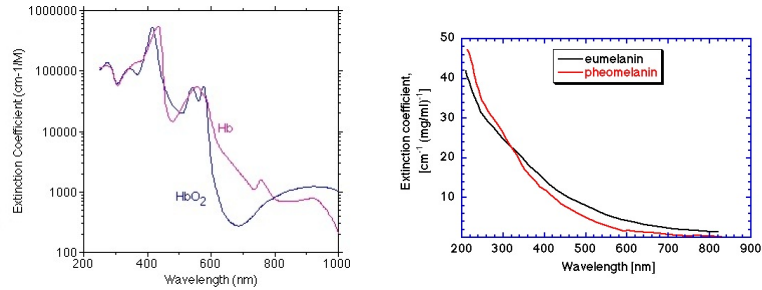


Figure 1.4: The optical absorption spectra of hemoglobin(left) and melanin(right). Note that the hemoglobin absorption spectrum is plotted on a semi-log scale. Image of hemoglobin spectra is credited to Scott Prahl and the image for melanin spectra is credited to Steven Jacques.

much interest in the detection of metastatic melanoma, or aggressive skin cancer, with the use of biomedical photoacoustic techniques. Such an application is only possible because of the over-expression of melanin in the average melanoma cell. McCormack *et al.* have demonstrated the ability to detect metastasis in sentinel lymph nodes (2009) and even single cells of metastatic melanoma (2011). Figure 1.4 shows the absorption spectra of hemoglobin and melanin. However, the large majority of tissues in the body are un-pigmented and inaccessible to optical photoacoustics without alteration.

There is a current need to develop consistent methods of photoacoustic labeling for un-pigmented cells so the success with the detection of blood and melanin can be translated to other parts of the body. Oraevsky *et al.* (2001) first suggested the use of gold and silver nanoparticles as contrast agents for the sake of photoacoustic tomography due to their high optical absorption and Mallidi *et al.* (2011) targeted nanoparticles to tissue *in vitro* for photoacoustic imaging. However, the current procedures are underdeveloped and have only been used to target tumors *in vitro* or in small animals. This method needs to be optimized and also translated for consistent single cell attachment for application in the photoacoustic flow cytometer.

1.5 Gold Nanoparticles

Gold nanoparticles, nanometer size particles of gold usually in suspension, have recently found widespread applicability in the medical field due their unique optical and metallic properties along with the relative ease of nanoparticle surface conjugation with molecular probes. The shape and size of the nanoparticles largely determines their optical properties. For instance, gold nanospheres (5-100 nm) suspended in water, or a fluid with similar dielectric characteristics, absorb light in the visible spectrum within the wavelength ranges from 520-580 nm (Daniel & Astruc, 2004). On the other hand, gold nanorods can be tuned in size to absorb within the wavelength ranges of 650-1500 nm while nanoshells can be tuned to absorb over the entire visible-NIR spectrum (400-1000 nm). These particles can be made into other shapes as well, e.g. cuboidal, hexagonal, etc., but the three noted above are the most common due to ease of fabrication and range of applicability.

The optical properties of nanoparticles are due the phenomenon of plasmon resonance, which are collective excitations of electrons on the nanoparticle surface due to light irradiation (Daniel & Astruc, 2004). The resonance of the surface electrons is highly dependent on the surrounding dielectric media. Therefore, the plasmon resonance is extremely sensitive to the local dielectric environment and the nanoparticle can be used to measure small changes in the surroundings through its optical properties. Figure 1.5 shows a cluster of spherical AuNPs under scanning electron microscopy and also the relative absorption of spectra of spherical AuNPs of different diameters suspended in water.

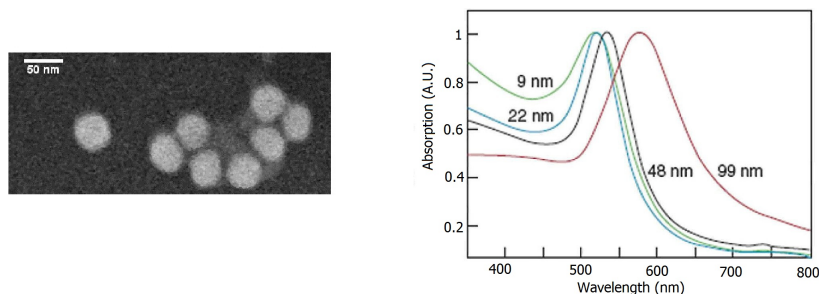


Figure 1.5: A scanning electron microscope image of 50nm gold nanoparticle with conjugated protein(left) and the optical absorption spectra of gold nanoparticle suspensions with different mean diameters as denoted on the graph.

1.5.1 Gold Nanoparticles in Photoacoustics

The photoacoustic effect requires light absorption, or pigmentation as applied to optical wavelengths, which is naturally present in melanoma in the form of melanin but is absent in most other cancers, including breast cancer. Nonetheless, photoacoustic flow cytometry was used to detect prostate cancer, one such non-pigmented cancer, by the attachment of gold nanoparticles (AuNPs) to the cancer cells via immunochemistry (Viator *et al.*, 2010). Since AuNPs have tunable and strong absorption peaks in the visible spectrum, they are valuable optical contrast agents which can be used to artificially pigment cells. This attribute is often exploited for photoacoustic imaging which reconstructs an image from the laser induced ultrasound. Breast and prostate cancer have both been targeted with AuNPs for photoacoustic imaging in mouse models (Zhang *et al.*, 2009b; Agarwal *et al.*, 2007). Other nanoparticles (NPs) like carbon nano-tubes or magnetic NPs have also been successfully used as contrast agents for photoacoustic imaging (Mallidi *et al.*, 2011).

Generally, these NPs can be targeted to cancer by functionalizing the surface of the NPs with amine or carboxyl groups and performing conjugation chemistry to join them with anti-bodies. These antibodies are chosen from those that readily bind

to cell surface antigens over-expressed on most tumorous cells. Anti-EGFR, -Her2, and -EpCam anti-bodies have been successfully bound to NPs and attached to breast cancer cells by various groups (Wang & Thanou, 2010; de Broek *et al.*, 2011; Acharya *et al.*, 2009; Kang *et al.*, 2009). Usually, the EDC zero-length cross-linker is used to bind the functionalized NP to the anti-body of interest before targeting the protein-NP-conjugate to the cell (Acharya *et al.*, 2009). Additionally, streptavidin-biotin mediated antibody-to-nanoparticle binding can also be used as biotin conjugated antibodies and streptavidin conjugated nanoparticles are commercially available. These methods can all be used to target circulating breast cancer cells in blood and deliver optical contrast specifically to the cells of interest.

1.6 Flow Cytometry

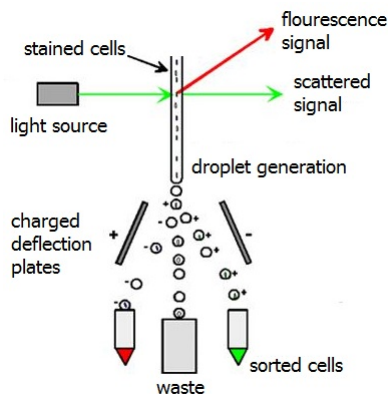


Figure 1.6: Cells flowing through a flow cytometer are measured according to their fluorescent and scattering signals which are used to sort them out as droplets with a charged deflection plate which can charge the droplets and attract them into one container or another.

Flow cytometry has been implemented in an attempt to detect and capture circulating breast cancer cells with some success (Takao & Takeda, 2010). A flow cytometer is generally a microfluidic instrument in which cells are illuminated as they

flow individually past a light source while an optical detector records both fluorescence and scattered signals emitted from the cell as a result of the interaction with the light source. Usually the cell is enhanced with a fluorophore attached to the cell membrane through immunochemistry (Givan, 2001). Though this system is capable of analyzing single cells, the sensitivity comes at a cost of sample size and speed of detection.

The microfluidic flow rates are 1-20 $\mu\text{L}/\text{min}$ and cells must be irradiated and analyzed individually or in very small groups. For instance, the general microfluidic channel width ranges from 30-100 μm which necessitates a slow rate of testing and small sample sizes to keep the duration of the test to a feasible length. Cell concentrations of 10^5 - 10^6 cells/mL are used because higher concentrations would confound results as multiple cells would be analyzed at the same time and their scattering and fluorescence signals would combine. Usually 30,000-40,000 cells would flow through the system at most since each cell would have multiple dimensions of fluorescence and scattering data stored resulting in a colossal amount of data (Givan, 2001). After detection, cells can be sorted by charging droplets with charged deflection plates (Figure 1.6).

1.7 Photoacoustic Flow Cytometry

Photoacoustic flow cytometry (PAFC) uses the photoacoustic effect to interrogate cells under flow and identify those of interest. Unlike fluorescent flow cytometry where a light signal is sent in and light signal (fluorescent emission) is detected, in PAFC a light signal is sent in and an acoustic/ultrasonic signal is detected. The benefit of photoacoustic cytometry over fluorescent cytometry is that thousands of cells can be interrogated at once with one laser pulse in PAFC, while cells need to be analyzed one-by-one in fluorescent cytometry.

Weight *et al.* (2006) have presented a method of photoacoustic flow cytometry specifically for the detection of circulating melanoma cells which can solve the problems encountered by traditional flow cytometry. In photoacoustic flow cytometry, cells in solution are irradiated as they flow past a pulsed laser while an ultrasonic detector senses the laser induced ultrasound generated by the cell due to light absorption as a result of the photoacoustic effect. The photoacoustic cytometry method is a significant advancement since up to 15 μL of sample can be irradiated and sensed at once without sacrificing single cell sensitivity to melanoma. Moreover, since a relatively large volume can be tested at once, flow rates on the order of 100-200 $\mu\text{L}/\text{min}$ can be used and large sample volumes can be tested faster than traditional flow cytometry. Moreover, thousands of cells can be analyzed with a single laser pulse since the photoacoustic effect will only be initiated by a pigmented cell.

McCormack *et al.* (2011) demonstrate single cell detection of melanoma cells suspended in 1X PBS with flow rates up to 250 $\mu\text{L}/\text{min}$ (phosphate buffered saline) under flow using an ultrasound imaging system as the photoacoustic transducer. The study shows the ability to detect 5-10 melanoma cells in 14 μL with a single pulse and differentiate them spatially in the flow chamber based on the time of arrival of the emitted acoustic wave to the acoustic transducer. Similar results were also found by Viator *et al.* (2010) with gold nanoparticle enhanced prostate cancer cells, however, an optical reflectance pressure sensor was used as the acoustic transducer. Moreover, Gutierrez-Jurez *et al.* (2010) claim to detect a single melanoma cell in 10^5 white blood cells with one laser pulse.

O'Brien *et al.* (2012) developed a method for capture of detected melanoma cells using two-phase flow where cell suspension and optical-grade mineral oil flow simultaneously into a single chamber. Since the two fluids are immiscible, they enter into the single chamber sequentially creating small volumes or 'slugs' (5-7 μL) of cell

suspension separated by volumes of oil. Each slug of cell suspension is tested by the laser beam which irradiates a $3\ \mu\text{L}$ volume. If the slug tests positive of the presence of a cancer cell, it is captured further downstream (Figure 1.7).

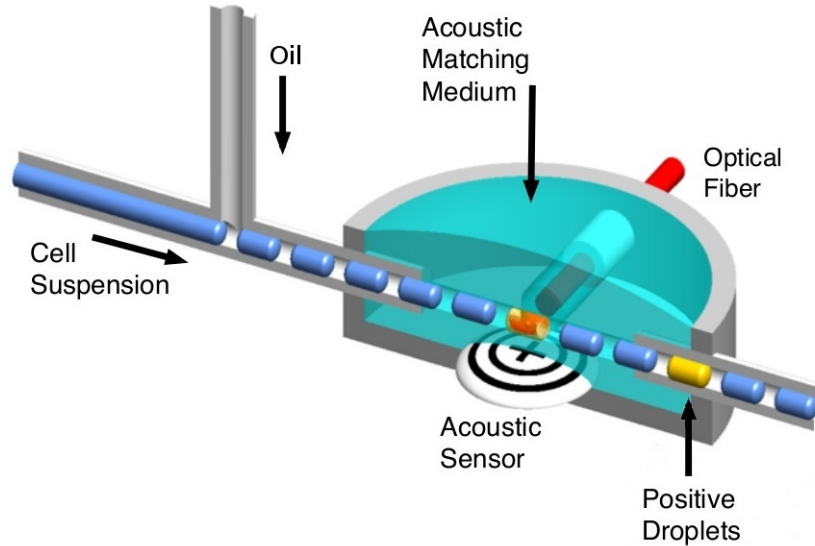


Figure 1.7: Cell suspension and oil flow simultaneously into a flow chamber and separate into droplets or slugs of each fluid. Each slug of cell suspension is tested by the laser and if it tests positive for cancer, the slug is collected downstream.

On the other hand, Zharov *et al.* (2006) have developed an *in vivo* photoacoustic flowmetry system which shows similar sensitivity to circulating tumor cells (CTCs) in mice models but the flow chamber is a blood vessel in the mouse ear. The volume that is irradiated by the laser is not reported but a single melanoma cell was detected amongst 10^6 other blood cells. However, the flow rate is unknown and variant with the heartbeat of the mouse. Though the *in vivo* photoacoustic flow cytometry method demonstrated robust detection for a nude mouse model, such success may be hard to replicate in humans because the total blood volume increases by about 10^3 fold and the melanin expression in skin could cause significant laser energy attenuation before it reaches the sub-dermal blood vessels. Moreover, the *in vivo* method does not allow the researcher to capture the detected cancer cell. The captured cell could

be genetically profiled which would allow clinicians to model drug therapy in order to target CTCs.

Chapter 2

Nanoparticle Conjugation and Detection of Breast Cancer Cells

A dual modality nanoparticle-antibody conjugate was made and targeted to breast cancer cells. This fluorescent-gold nanoparticle was created so the attachment of the optically absorbing gold nanoparticles could be verified with fluorescent microscopy of live cells. The optical absorption of the gold nanoparticles was largely responsible for the generation of the photoacoustic (PA) wave. A specific concentration of nanoparticle tagged breast cancer cells suspended in saline was tested with the photoacoustic flow cytometer (PAFC) to determine the detection limit of the system without any background. Time and frequency domain features were identified in order to aid in automated classification of cancer cells under flow.

2.1 Nanoparticle Analysis and Antibody to Nanoparticle Conjugation

2.1.1 Optical Properties of the Nanoparticles

Gold nanoparticles (AuNPs) were used because of their tunable optical absorption, allowing for peak absorption near the harmonic laser wavelength of 532 nm. Spherical gold nanoparticles 54 nm in diameter purchased from Nanopartz Inc. (Loveland,

CO) at a concentration of 5×10^{12} nanoparticles/mL was tested with an Ocean Optics HR200 High Resolution Spectrometer to verify optical absorption profile.

Photoacoustic spectra measurements were made with the set up described in Figure 2.1. An Nd:YAG Q-switched laser with a 5 ns pulse and an OPO which allowed laser wavelength tunability from 420-2400 nm was used to irradiate the AuNP sample. Stock AuNP solution of $4 \mu\text{L}$ was used as sample and tested from 480-570 nm in 10 nm increments. The radiant exposure at each wavelength ranged from 10-15 mJ/cm^2 . The peak-to-peak voltage (V_{p-p}) divided by the radiant energy of the irradiating wavelength was used as a measure of absorption. Both spectrometric and photoacoustic measurements were normalized by division of all values by the highest absorption value in each mode of measurement for the sake of simple comparison between both methods.

Figure 2.2 demonstrates the AuNP solution has an absorption peak somewhere between 530-540 nm since the spectroscopic and photoacoustic measurements are in good agreement. This demonstrates that the PA emission at the 532 nm harmonic wavelength will be robust and can be used for the rest of study. Though a tunable laser was available, using a harmonic wavelength like 532 nm has benefits, as all of the findings from this study can be easily translated to a cheaper Q-switched laser system which works only at that wavelength. This allows the research to be more translatable when the times comes.

Furthermore, the concentration dependent extinction coefficient of the gold nanoparticles were determined through traditional spectrometry. The absorption coefficients of seven incrementally increasing concentrations of AuNP suspension at 532 nm were measured. The slope of the line of best fit (R-squared = 0.98) was used to determine concentration dependent extinction coefficient of $5 \text{ cm}^{-1}/10^{11}$ AuNPs/mL.

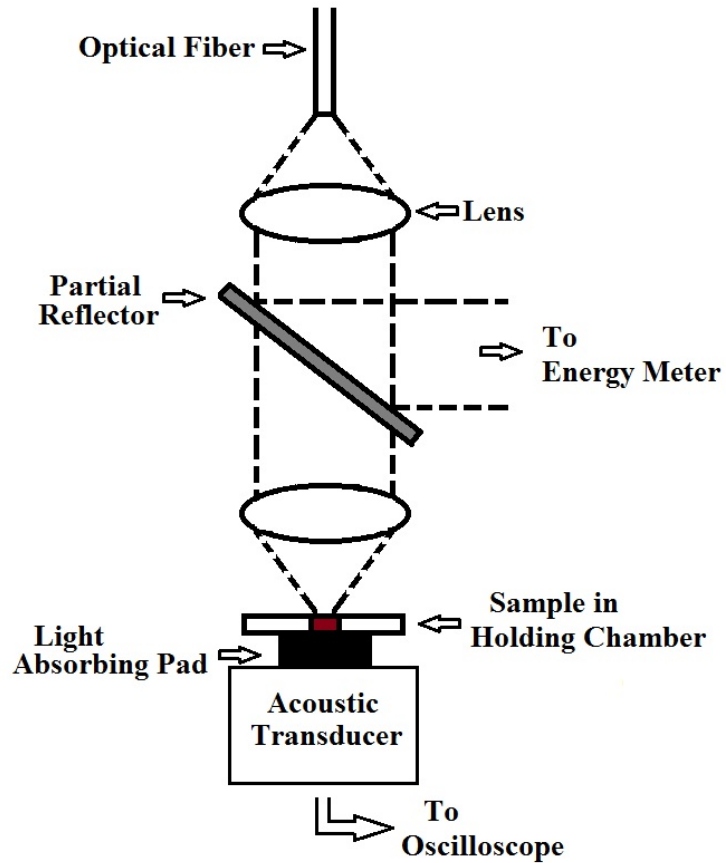


Figure 2.1: Set up used to take photoacoustic spectra measurements for the gold nanoparticles. Light is delivered from an optical fiber into a converging lens which collimates the light. A partial reflector reflects 5% of the light energy to an energy meter to measure radiant energy for every pulse. The remaining energy is re-focused into the suspension of AuNPs, generating a detectable photoacoustic wave. The light absorbing pad absorbs the remaining light and protects the acoustic transducer from light irradiation. The generated PA emission is detected by the acoustic transducer and sent to an oscilloscope.

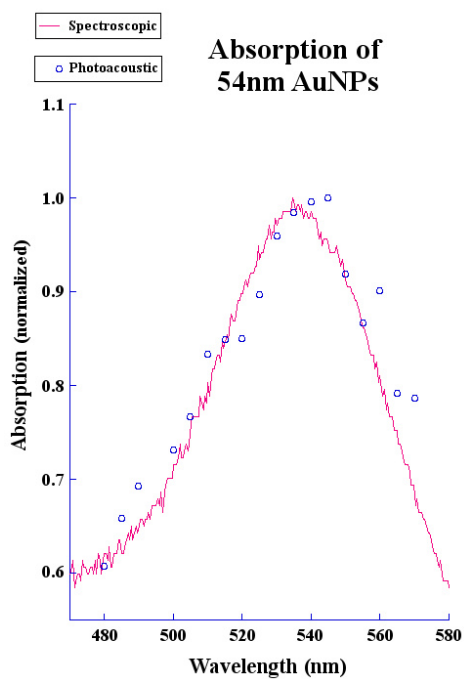


Figure 2.2: The optical absorption spectrum of 54 nm gold nanoparticles as found by traditional spectrophotometry (solid line) and through photoacoustic measurement (empty circles). This demonstrates the photoacoustic signal is essentially a measure of light absorption.

2.1.2 Conjugation Protocol

First, 45 μL of streptavidin coated 320 nm red fluorescent (TRITC) latex nanoparticles (Bangs Laboratories, Fishers, IN) were added to 1.5 μL of biotin conjugated anti-EpCAM monoclonal antibody (Pierce Antibodies, Rockford IL) in 1 mL of 1X PBS. This suspension was incubated at 22°C for 1 hour. Then 20 μL of Neutravidin conjugated 54 nm spherical gold nanoparticles was added to the suspension with an additional 500 μL of 1X PBS and allowed to incubate for 20 minutes. Finally, 1.5 μL of anti-EpCAM in another 500 μL of 1X PBS was added to the suspension and allowed to incubate for 30 minutes. The resulting suspension was centrifuged at 550 $\times g$ for 8 minutes in order to pellet the nanoparticles and leave the excess antibodies in suspension. The supernatant was removed and the nanoparticle pellet was resuspended in 1 mL of 1X PBS.

While it may seem that the volume and amount of analytes in the previous protocol are arbitrary, this is not the case. As a similar protocol has not been developed before by other researchers, all values had to be derived through theoretical calculations and experimentation. Please find a thorough review of the methods used in the Appendix A.

Fluorescent-gold nanoparticles were imaged with a scanning electron microscope (SEM) to ensure the expected results were achieved with the conjugation chemistry. Figure 2.3 show images of the fluorescent-gold nanoparticles demonstrating that the protocol described previously was successful in attaching the gold nanospheres to the larger fluorescent latex particles. Figure 2.3b demonstrates that clusters of particles also formed which were on the 1 μm scale.

Lowering the concentrations of analytes in the reaction could reduce the size and formation of these large clusters. However, these clusters may actually work to the

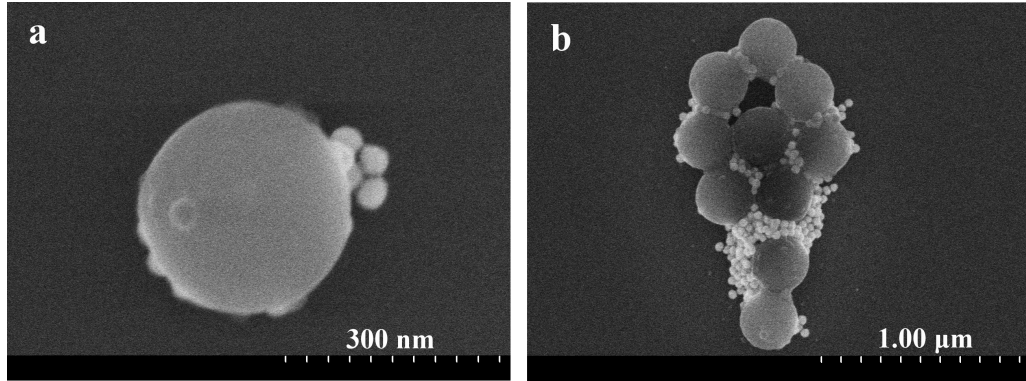


Figure 2.3: SEM images of fluorescent-gold nanoparticle. a) Image of a single fluorescent sphere with multiple, smaller gold spheres attached. b) Image of a cluster of fluorescent and gold spheres.

benefit of the researchers as they provide large, concentrated doses of optical contrast to the cell. Moreover, from an acoustic standpoint, the 20 MHz transducer being used is unable to resolve and differentiate between ultrasound signals emitted from these larger clusters as opposed to single groups since they are both at or below $1\ \mu\text{m}$. Therefore, the presence of clusters should not change the detected frequency components of the PA signal. A more thorough analysis of photoacoustic signal frequency components will be done later in the chapter.

2.2 Nanoparticle Attachment to Cancer Cells

Cultured T47D breast cancer cells were diluted into a concentration of 10^6 cells/mL in 1 mL of 1X PBS and incubated with $80\ \mu\text{L}$ of the fluorescent-gold nanoparticle suspension created in Section 2.1.2. This solution was allowed to incubate for 30 minutes and then centrifuged at $140\times g$ for 10 minutes to remove excess nanoparticles. The cell pellet was resuspended in 1 mL of 1X PBS.

The control group of cells with 10^6 cells/mL in 1 mL of 1X PBS was incubated with $1\ \mu\text{L}$ of stock anti-EpCAM solution for 30 minutes to block all EpCAM receptors and

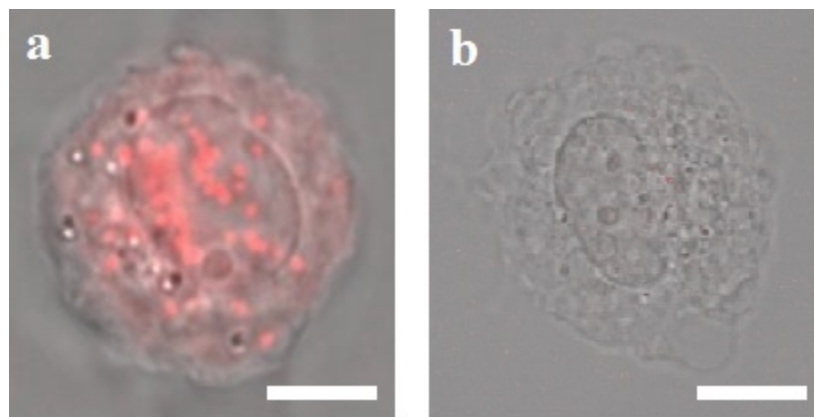


Figure 2.4: This image compares (a) a nanoparticle tagged cell and (b) a receptor blocked cell where all of the EpCAM receptors and even non-specific binding sites were blocked by previous incubation with anti-EpCAM before incubation with antibody-conjugated nanoparticles. Scale bar is $4\ \mu\text{m}$.

also the non-specific binding sites. After 30 minutes, the excess antibodies were cleaned out of suspension through centrifugation at $140\times g$ for 10 minutes. The cells were then resuspended in 1 mL of 1X PBS and incubated with $80\ \mu\text{L}$ of the fluorescent-gold nanoparticle suspension for 30 minutes. Since the EpCAM receptors on the cell surface had been blocked by previous incubation anti-EpCAM, no nanoparticles were expected to attach to the cell. After 30 minutes, the solution was centrifuged at $140\times g$ for 10 minutes in order to remove excess nanoparticles. The cells were then resuspended in 1 mL of 1X PBS.

These two cell suspensions, nanoparticle labeled and receptor blocked, were then prepared on a slide and imaged with an Zeiss LSM 510 Meta Confocal Microscope with a 40X water objective. The TRITC filter was used to view the emission from the fluorescent-gold nanoparticle. All images are reconstructed from acquired z-stacks where each stack was spaced by $0.5\text{-}1\ \mu\text{m}$ depending on the image.

As seen in Figure 2.4, the nanoparticles failed to attach to the receptor blocked cell (Figure 2.4b) while it attached quite well to the cell in 2.4a, from the unblocked group. This demonstrates that the nanoparticles were indeed targeting the EpCAM

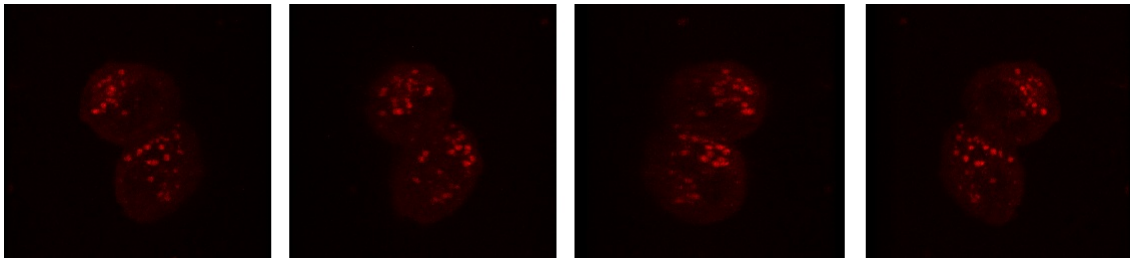


Figure 2.5: A montage of 3D reconstruction of a confocal z-stack. A $12\ \mu\text{m}$ deep stack with an image every $1\ \mu\text{m}$ was used to collect the data.

receptors on the cancer cell. This fact was important to verify as the nanoparticles themselves, without the help from the antibody, could have been attracted to some structures on the breast cancer cell. However, this is not the case, as indicated by the previous findings.

There is a diffuse red fluorescence as well as higher intensity localizations of fluorescence. This is due to the single and clusters of nanoparticles as shown in Figure 2.3. This single particle in Figure 2.3a is not optically resolvable; however, the larger cluster in Figure 2.3b is since it is on the order of $1\ \mu\text{m}$.

A lot of the nanoparticles have been internalized by the cell but this is better visualized in Figure 2.5. This figure is 4 frames out of a 3D reconstruction of a confocal z-stack image of two nanoparticle tagged breast cancer cells. These experiments demonstrate that the nanoparticles did attach to the cell and could therefore, provide artificial optical contrast. The internalization of nanoparticles does pose some pertinent questions, since the cell replaces the EpCAM receptors on the membrane after endocytosis of the ones with nanoparticles attached. However, this does not seem to be the case for the receptor blocked cells during the time scales for which they were exposed to the nanoparticle suspension.

2.3 Black Microspheres as Cancer Cell Phantoms

The sensitivity of the photoacoustic flow cytometer (PAFC) is first standardized using $10\ \mu\text{m}$ black latex spheres since they are man-made materials which can be synthesized with little variance. However, this consistency also makes them limitedly comparable to biological cells which are of variable sizes with differing amounts of proteins, like EpCAM, and therefore, with different amounts of nanoparticles. Nevertheless, the photoacoustic responses from different concentrations of $10\ \mu\text{m}$ spheres aid in the development of signal processing methods which were translated with modification to biological cells. After initial testing with $10\ \mu\text{m}$ microspheres, breast cancer cells were tagged with nanoparticles and tested with the PAFC system under similar conditions. Signals were processed using techniques developed from the black microsphere testing and results were compared in order to draw conclusions about the sensitivity and efficacy of the system.

The general *in vitro* flow technique is described in Section 1.7 and shown in Figure 1.7. The flow chamber was cylindrical with a width of 1.5 mm. It was made of $10\ \mu\text{m}$ thick quartz glass which was thin enough to allow for acoustic coupling into the acoustically matched medium. The laser wavelength of irradiation was 2.5 mJ at 532 nm resulting in an approximate radiant exposure of $100\ \text{mJ}/\text{cm}^2$ at the chamber and irradiating $3\ \mu\text{L}$ of fluid with one laser pulse. The analog PA signal was amplified 32 dB and filtered with a bandpass filter from 1-50 MHz. The digitized data was not averaged and collected with a time resolution of 1 ns and a $800\ \mu\text{Volt}$ voltage resolution.

2.3.1 Microsphere Tests

Two concentrations of $10\ \mu\text{m}$ spheres suspended in saline were made so that under flow the expected number of spheres being irradiated every time was either 2 or 4, exclusively for each concentration. If the expected value is known, then the probability of the occurrence of any integer value can be approximated through the Poisson Distribution (Tables 2.1 and 2.2). For each group, the sum of all probabilities shown on the table is greater than 99% implying that these events are the most likely to occur.

Table 2.1: Expected Value of 2 Events

Spheres Irradiated	Probability
0	0.135
1	0.271
2	0.271
3	0.180
4	0.090
5	0.036
6	0.012

Table 2.2: Expected Value of 4 Events

Spheres Irradiated	Probability
0	0.018
1	0.073
2	0.147
3	0.195
4	0.195
5	0.156
6	0.104
7	0.059
8	0.029
9	0.013

Using these two concentrations it is possible to determine the detection limit of the PAFC system in terms of the number of spheres. Signals from these two sets were

compared with the signals from the negative control of pure saline without any microspheres. The signals from the entire flow chamber was first compared to determine which waveforms contained distinguishable signals from microspheres. Then signals within those select waveforms were further analyzed to determine the best processing algorithm which allowed for the highest signal to noise ratio. Finally, all processing is repeated with modifications and signals are re-analyzed to determine the detection limit.

2.3.2 Global Analysis of Entire Flow Chamber

A total of 31 waveforms measuring PA response were acquired for each of the three groups: saline, 2 spheres/pulse, and 4 spheres/pulse. Since the chamber is 1.5 mm wide and the speed of sound in water is 1.5 mm/ μ sec, the voltage signal from the acoustic response from within the chamber lasts 1 μ sec. With a sampling rate of 1 ns, each waveform is composed of 1000 points.

Initially, only one feature was used to determine which waveforms from the 2 and 4 spheres/pulse groups contained signals from microspheres. The feature was computed by squaring every element of the waveform and summing them together. This would make all values positive and emphasize peaks corresponding to PA responses.

$${}^2f = \sum_{n=1}^{1000} F_n^2 \quad (2.1)$$

Where F is a waveform and F_n is the n^{th} element in that waveform. This 2f value was computed for every waveform in each group. Only those waveforms from the 2 and 4 spheres/pulse groups which had 2f values 2.5σ greater than the mean squared integral from the saline signals were considered to have signals from microspheres. This method of classification was fairly harsh and exclusive, since it was qualitatively

clear after plotting excluded waveforms that it dismissed some which had signals in them.

This classification technique determined that 32% of the waveforms from the 2 spheres/pulse had signals from microspheres. When compared to the ideal result indicated by the Poisson distribution of 86%, since about 13.5% would have no spheres, this is fairly bad. It places the detection limit at about 3 microspheres since there is approximately a 32% chance of there being 3 or more microspheres in the chamber. However, this was just a cursory classification procedure in order to identify more features from PA signal analysis from those waveforms which it classified as containing microsphere signals.

2.3.3 Microsphere Signal Analysis

Signals from microspheres lasted for 50-100 ns. Figure 2.6a is the voltage trace of a PA signal from a microsphere as compared to noise. Both were extracted from an entire PA signal from the whole chamber which is composed to 1000 ns or 1000 points. Over 30 such signals were selected from waveforms which were identified as having PA signals from microspheres. The FFT was used to calculate the power spectrum of the signals from the microspheres and also from the noise traces. A 100 ns window containing the PA signal or a sample of noise was used for the transformation. Since the 1 ns sampling rate limits the Nyquist frequency to 500 MHz, a trace with 100 points or 100 ns will allow for a 10 MHz frequency resolution with the FFT due to the symmetrical nature of the transformation which, in this case, has 50 points of resolution.

The power spectrum of each PA signal was calculated by multiplying the complex number by its conjugate for each frequency. This was done for both the microsphere signals and the noise signals. An average power spectrum was calculated for each

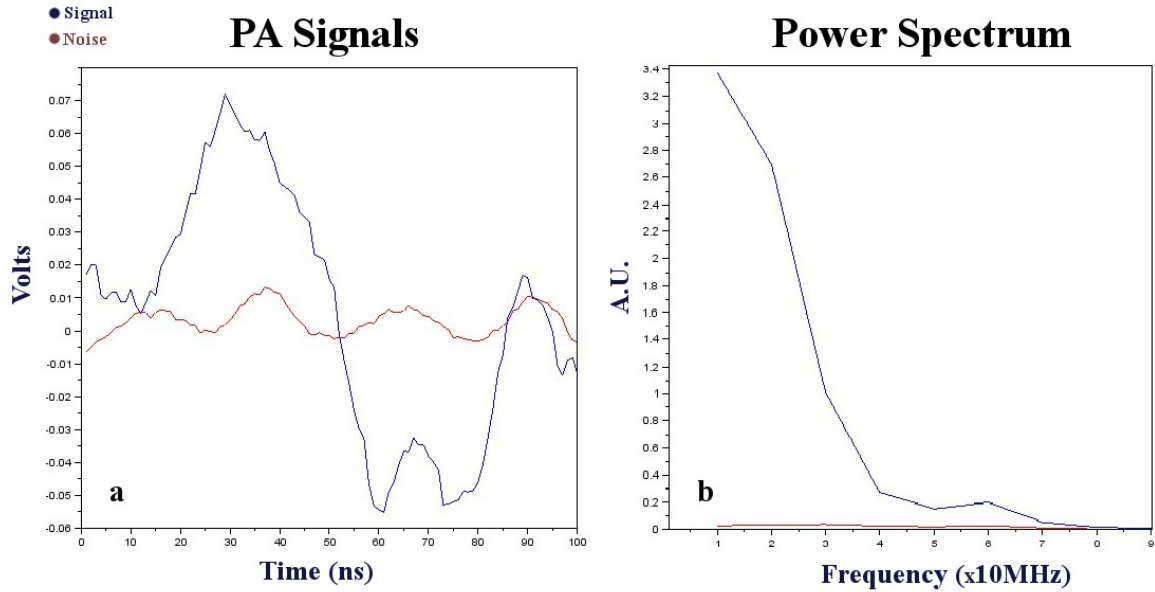


Figure 2.6: a) Voltage trace of a PA signal from a microsphere (blue) as compared to that of noise (red). b) Average power spectrum of PA signal from microspheres (blue) and noise (red). Notice that the power spectrum from the noise is exceptionally small when compared to that of the signal.

group and is plotted in Figure 2.6b. The power spectrum of the PA signals of the noise is very small compared to that of the microspheres. Though they are both largely composed of the same frequencies, there is a difference in how the power is distributed between all of the frequencies for signals from microspheres as opposed to noise. Figure 2.7 is a plot of how the contribution from each frequency brings the signals closer to its total power which has been scaled to 1 for both, microspheres and noise.

The largest component of the signals from microspheres are before 30 MHz, since by 30 MHz the amount of power in the signal has already reached above 0.9 or 90% of its final value. By comparison, the noise signals have reached 0.65 or 65% of the final value. It is interesting to note that though all signals were filtered at 50 MHz, about 25% of the power for the noise is in higher frequencies.

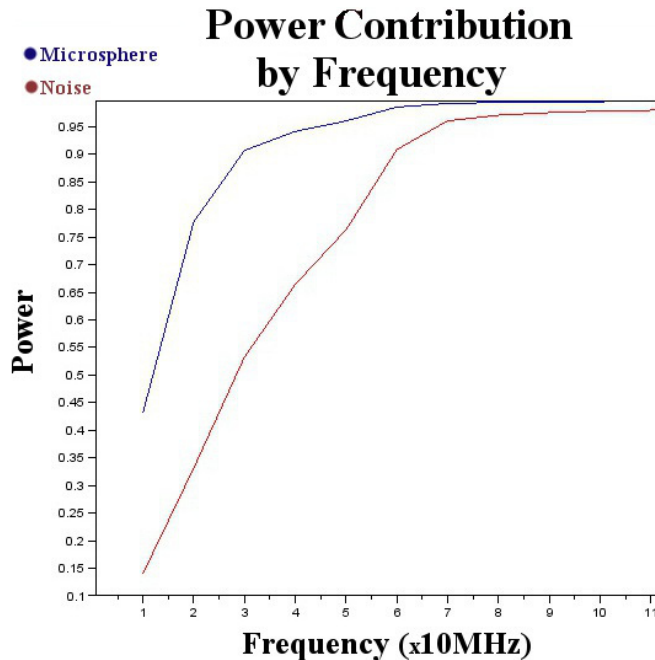


Figure 2.7: Plots the incremental contribution of each frequency to the total power of the PA signals from microspheres and noise. Total power has been scaled to 1 for both groups for easy comparison.

Using this information we can develop a computational low-pass filtering technique which can further increase the signal to noise ratio in the time domain by accepting the majority of the power from the microsphere signals and rejected a large portion of the power in the noise. For instance, by low-pass filtering at 30 MHz we could increase the SNR for the average microsphere signal by $(0.9/0.65)$ or 1.38 times. By low pass filtering at even lower frequencies, like 10 MHz, we could potentially increase the SNR by up to 2.7 times.

2.3.4 Re-Analysis of Entire Flow Chamber

The motivation for these processing techniques is to identify a method which can analyze the entire chamber and indicate the presence of an absorber. Therefore, apart from analyzing single PA responses from microspheres within the chamber, the entire

chamber also needs to be further analyzed in order to find distinguishing features.

A new time domain feature was identified which counted the number of points in a waveform above some noise threshold which was calculated from the control signals from saline. First, the average fluctuation of the noise from 0 mV was calculated by averaging the absolute value of every element in every waveform in the saline group (Equation 2.2). Then the standard deviation of the fluctuation in the noise was calculated for the absolute value of every element in every waveform in the saline group (Equation 2.3). Finally, the noise value or threshold was calculated using the average fluctuation and standard deviation, Equation 2.4. The number of points above this threshold in the absolute value any waveform is a feature (Equation 2.5).

$$\bar{N}_0 = \frac{1}{1000M} \sum_{k=1}^M \sum_{n=1}^{1000} |F_n^k| \quad (2.2)$$

$$\sigma_{N_0} = \frac{1}{1000M} \sqrt{\sum_{k=1}^M \sum_{n=1}^{1000} (|F_n^k| - \bar{N}_0)^2} \quad (2.3)$$

$$\vartheta = \bar{N}_0 + 2.5\sigma_{N_0} \quad (2.4)$$

$$^{N_0}f = \sum_{n=1}^{1000} \text{ceiling}((|F_n^k| - \vartheta) + ||F_n^k| - \vartheta|) \quad (2.5)$$

Equations Specifics: $|F_n^k|$ is the absolute value of the n^{th} element in the k^{th} waveform. Each waveform is composed of 1000 elements and M is the total number of waveforms. The threshold value in Equation 2.4 is $2.5\sigma_{N_0}$ away from the average fluctuation due to noise. Finally, the operation in Equation 2.5 on the right of the summation results in a 1 when a point is above threshold and 0 when it is below.

These two features, values above noise(^{N_0}f) and squared integral(2f), were used for classification after all signals were computationally filtered with a bandpass of 1-30 MHz. This frequency range was chosen because other ones resulted in poor

classification by dismissing signals from microspheres which were sharp and composed of higher frequencies.

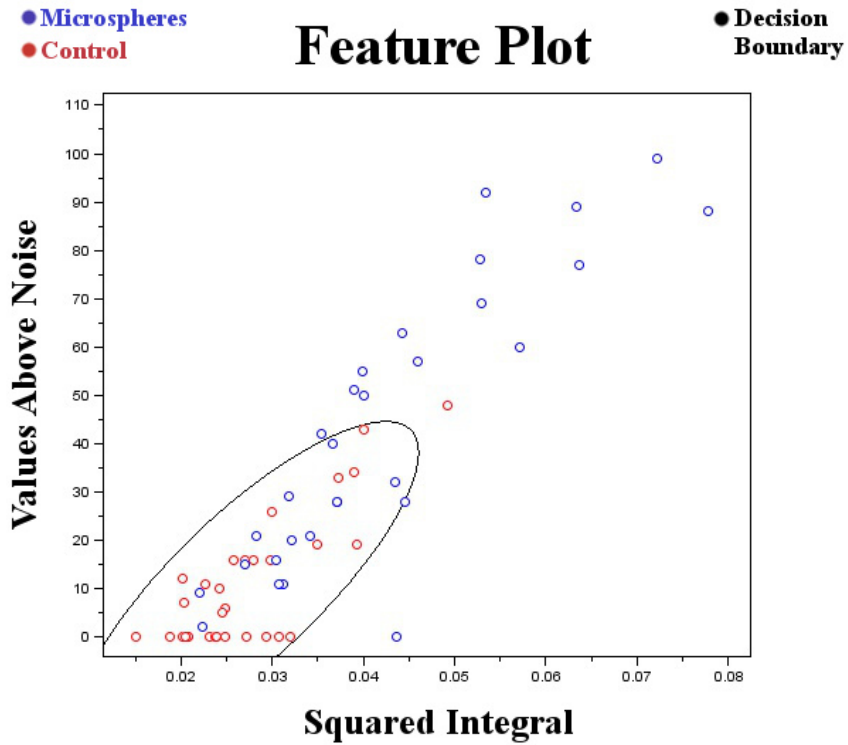


Figure 2.8: Each waveform from the 2spheres/pulse group(blue) and the saline group(red) is plotted as a point in feature space. The black boundary is a threshold (2.5σ) determined by the bivariate gaussian parameters of the control/saline distribution.

Figure 2.8 is a plot in feature space of each waveform from the 2 spheres/pulse group (blue) and the saline group (red). A threshold was used as the classification boundary by assuming that the control or saline feature distribution was bivariate normal. A circle centered around the origin with a radius of 2.5 was transformed into the ellipse with Equation 2.6.

$$Ellipse = \Phi\Lambda^{\frac{1}{2}}Circle \quad (2.6)$$

Where Λ are the eigenvalues of the covariance matrix of the saline feature distribution

and Φ are the eigenvectors. This is called unwhitening or coloring the standard bivariate normal distribution.

In Figure 2.8, the one point outside of the boundary from the saline group had a noticeable PA signal from some absorber, likely a contaminant. One point from the microsphere group was excluded from the graph since it contained a very large PA signal and therefore, had large values for both features. There are 17 points from the microsphere group which are outside of the boundary, meaning 55% of the 2 spheres/pulse waveforms were correctly classified as being different from the control.

The Poisson distribution indicates that for the 2 spheres/pulse expected value there are 2 or more microspheres in the chamber 60% of the time. Keeping in mind that there is a 10-20% chance of a microsphere getting 'lost' in the flow system, a classification rate of 55% is a fairly good indication that the detection limit is at least 2 microspheres. This is a marked improvement over the original 32% classification and 3 microspheres detection limit.

This classification technique will now be modified and replicated on breast cancer cells.

2.4 Breast Cancer Cell Tests

A similar procedure was followed to test the breast cancer cells, since waveforms from 2 cells/pulse and 4 cells/pulse were compared with waveforms from just saline. The cancer cells were first targeted with the nanoparticles and then tested with the cytometer under these two concentrations. Signal filtering frequencies were identified and the same features were used to classify waveforms with signals from cancer cells.

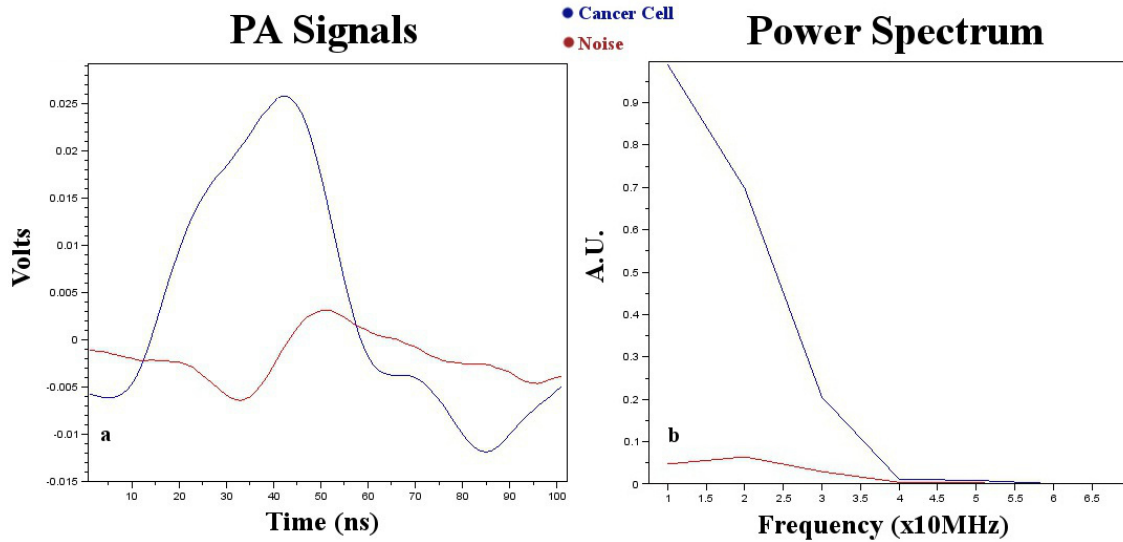


Figure 2.9: a) Voltage trace of a PA signal from a cancer cell (blue) as compared to that of noise (red). b) Average power spectrum of PA signal from cancer cells (blue) and noise (red).

2.4.1 Breast Cancer Cell Signal Analysis

Signals from single cells last 50-100 ns in duration, making them comparable to signals from $10\ \mu\text{m}$ spheres. The photoacoustic contrast agents in the breast cancer cells are nanoparticles which have been attached with immunochemistry as opposed to the homogeneous dye which was present in the microspheres. Though theoretically each nanoparticle should emit a high frequency acoustic wave with a principle component wavelength on the order of nanoparticle diameter, stress confinement issues convolute this signal. During the 5 ns laser pulse, acoustic waves travel $7.5\ \mu\text{m}$ in water, making the resolution limit of this technique on that order or worse. Therefore, the signals emitted by breast cancer cells with nanoparticles are very similar to those emitted by $10\ \mu\text{m}$ black microspheres with homogeneous dye.

Figure 2.9 was created with same techniques used to create Figure 2.6.

Similar frequencies compose both the noise and the signals from the cancer cells

making it difficult to identify a characteristic frequency band. Moreover, analysis of the incremental power contribution from each frequency reveals the further issue that cancer cell signals and noise signals have a similar distribution of power across all component frequencies. Figure 2.10 demonstrates that when the total power is normalized to 1 for both cancer cell signals and noise, the incremental power added by each frequency is about the same. From this, one can infer that filtering will not increase signal-to-noise ratio significantly.

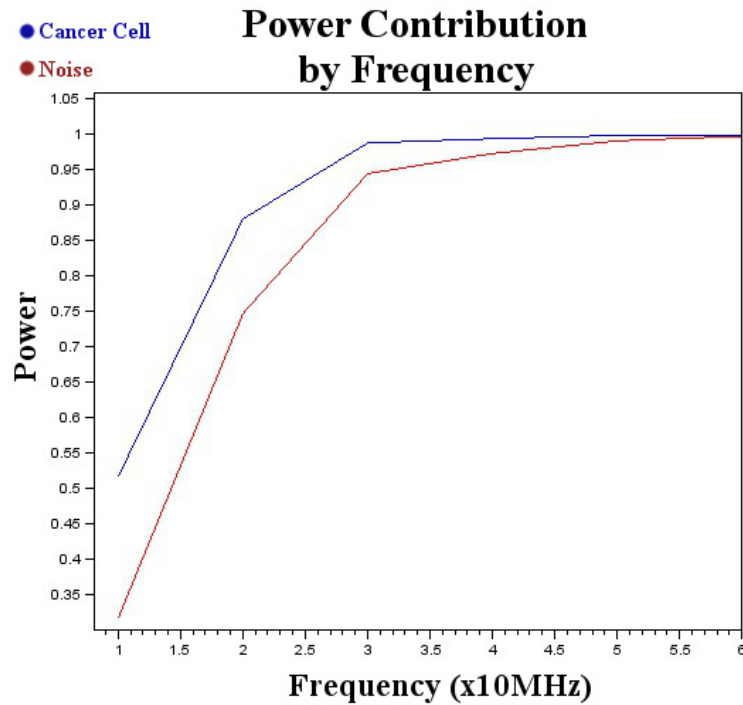


Figure 2.10: Plots the incremental contribution of each frequency to the total power of the PA signals from cancer cells and noise. Total power has been scaled to 1 for both groups for easy comparison.

However, it should be noted that the power contribution by each frequency for the noise was different in this case when compared to the tests which were completed for the microsphere study. There is no reason for these two to be different unless there was some contaminant within the saline which emitted low energy, below threshold

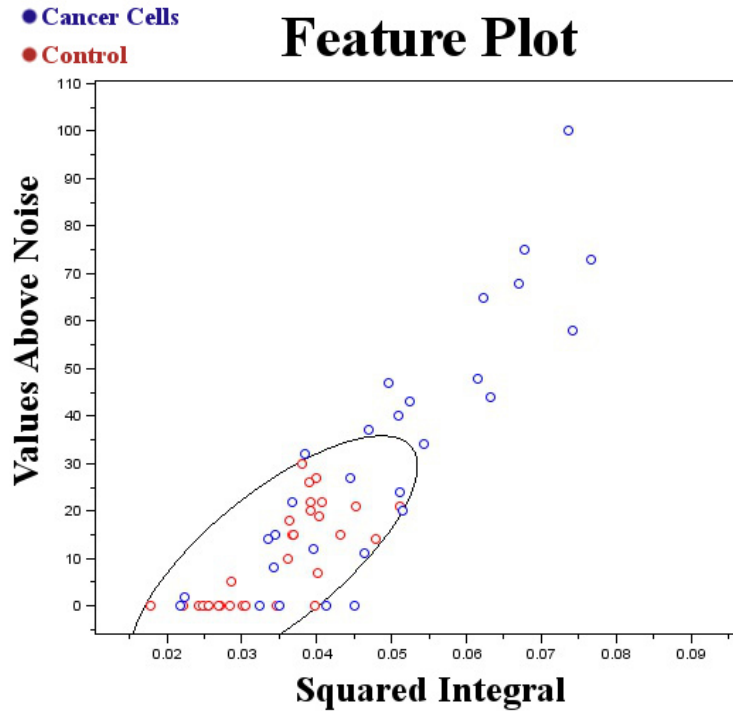


Figure 2.11: A feature space plot of the 2 cells/pulse (blue) and saline group (red) where each waveform is plotted as a point. The black line is the 2.5σ boundary of the saline group distribution, assuming it is bivariate normal.

acoustic waves which changed the noise frequency profile but did not effect the magnitude of the background noise. For these reasons, a filtering technique should not be dismissed because it may still increase the signal-to-noise ratio for cancer cell PA emissions.

2.4.2 Breast Cancer Cell Detection Limit

Waveforms from the entire chamber were computationally filtered from 1-30 MHz. The squared integral and values above the noise features, as described by Equations 2.1 and 2.5, respectively, were extracted from each waveform. Figure 2.11 plots each waveform as a point in feature space from both the saline and 2 cells/pulse group. The decision boundary was calculated using Equation 2.6.

There are a lot of similarities between this feature plot and the feature plot from the microsphere tests in Figure 2.8. The control or saline features from both tests fall within the same distribution and the decision boundary is nearly the same for both tests. This is a strong indication that the features being extracted are consistent and do not change from one test to the next, even over multiple days. Moreover, the features from the microsphere and cancer cell waveforms also seem to show the same general trend. These results demonstrate that microspheres are a sufficient alternative in lieu of cancer cells, validating the initial part of this study.

One point from the 2 cells/pulse group was omitted from Figure 2.11, since it had large values for both features and expanded the scales of the graph to a field-of-view too large to resolve the rest of the points. There are 15 points in the 2 cells/pulse group outside of the decision boundary making the classification rate 50%. Due to the Poisson distribution, this indicates a detection limit of about 2 cancer cells, meaning that at least 2 cancer cells must be present in the irradiated volume to generate a distinguishable PA signal.

Chapter 3

Breast Cancer Cell Detection in Saline and from Normal Blood

Breast cancer cells are targeted with nanoparticles through immunochemistry in order to provide pigment. After which, the PAFC device is calibrated to demonstrate a near single-cell detection limit. Cultured breast cancer cells are pre-labeled with DAPI and nanoparticles. Then they are added to whole blood to reach a biologically relevant concentration of about 25-45 breast cancer cells per 1 mL of blood. An *in vitro* photoacoustic flow cytometer is used to detect and isolate these cells followed by capture with the use of a micromanipulator.

3.1 PAFC Detection

The *in vitro* two-phase PAFC system is composed of two programmable syringe pumps (Braintree Scientific, Braintree, MA), one with optical grade mineral oil (Fisher Scientific) and the other with the prepared cell sample to be tested. Both fluids were pumped at 20 $\mu\text{L}/\text{minute}$ simultaneously into a 1.5 mm, 10 μm thick quartz flow chamber, creating alternating slugs of cell sample and oil, each approximately 7 μL in volume. A 1 mm optical fiber delivered 5 ns, 532 nm pulsed light transversely to a portion of the chamber. The laser irradiated 3 μL of fluid with every pulse and the radiant exposure at the chamber was approximately 125 mJ/cm^2 . An acoustic

transducer with a 20 MHz bandwidth (Olympus, Waltham, MA) was coupled with the irradiated portion of the flow chamber to capture the PA emission. The analog signal was amplified 50 dB (Ritec Inc., Warwick, RI) and digitized with a LabVIEW integrated PXI card (National Instruments, Austin, TX). The time resolution was 1 ns and the voltage resolution was $400 \mu\text{V}$.

3.2 Nanoparticle Attachment to Breast Cancer Cells

Cultured T47D breast cancer cells were diluted into a concentration of 10^5 cells/mL in 1 mL of 1X PBS and incubated with $10 \mu\text{g}/\text{mL}$ of DAPI for 10 minutes in order to label the cancer cell nuclei for easy identification. Then the cell suspension was centrifuged at $140 \times g$ for 10 minutes in order to remove the excess DAPI. The supernatant was removed and the breast cancer cell pellet was resuspended in 1 mL of 1X PBS. After which, $80 \mu\text{L}$ of the dual-modality nanoparticle suspension, described in Section 2.1.2, was added to the previously mentioned cell suspension. This solution was allowed to incubate for 1 hour and then centrifuged at $140 \times g$ for 10 minutes to remove excess nanoparticles. The cell pellet was resuspended in 1 mL of 1X PBS.

3.3 Cell Preparation

Breast cancer cells were tagged with nanoparticles using the same parameters as defined in Section 3.2. Then they were diluted into a concentration of approximately 670 cells/mL in 1 mL of 1X PBS. For this concentration of cells, approximately 2 cells are expected to be irradiated with each laser pulse, since $3 \mu\text{L}$ is the irradiated volume. This suspension was tested with the PAFC under the flow parameters previously described.

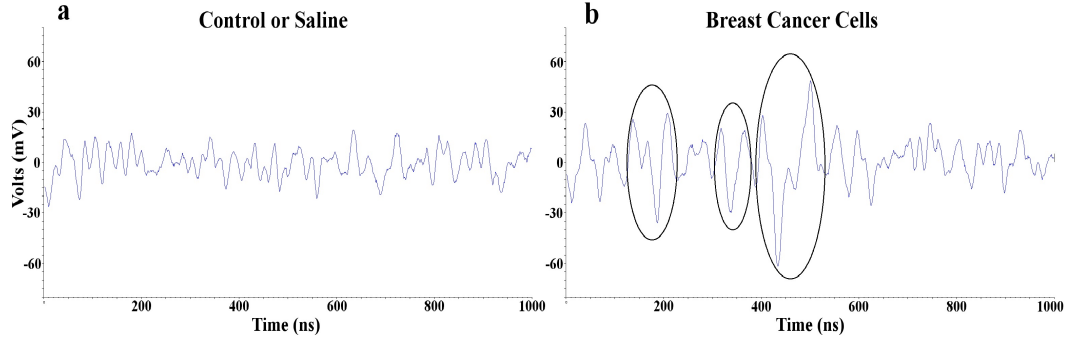


Figure 3.1: (a) Plot of photoacoustic waveforms acquired during the PAFC test from laser irradiation of just saline and (b) with nanoparticle tagged breast cancer cells at a concentration of $2 \text{ cells}/3 \mu\text{L}$. The three circles in part b designate three signals from three separate cells in the chamber.

3.4 Classification in Saline

The PA signals captured with each irradiation was x-y data with time and voltage values corresponding to acoustic pressure arriving at the ultrasound transducer at that moment. The chamber lasted $1 \mu\text{sec}$ in time since it was 1.5 mm in diameter and the speed of sound in water is $1.5 \text{ mm}/\mu\text{sec}$. Figure 3.1a shows a plot of the PA signal from within the chamber when there is just saline and 3.1b shows a PA signal from within the chamber when there are tagged breast cancer cells.

Two separate samples were tested with the PAFC system: saline and tagged breast cancer cells in saline at a concentration of $2 \text{ cells}/3 \mu\text{L}$. The photoacoustic waveform captured for each irradiation was saved and two features were extracted in post-processing. One feature was the integral of the PA signal from within the flow chamber after every value was squared. This integral was adjusted by subtracting from it the squared-integral of a portion of the voltage trace outside of the chamber which was considered noise. The basic calculation is described in Equation 2.1 but the value was adjusted for noise.

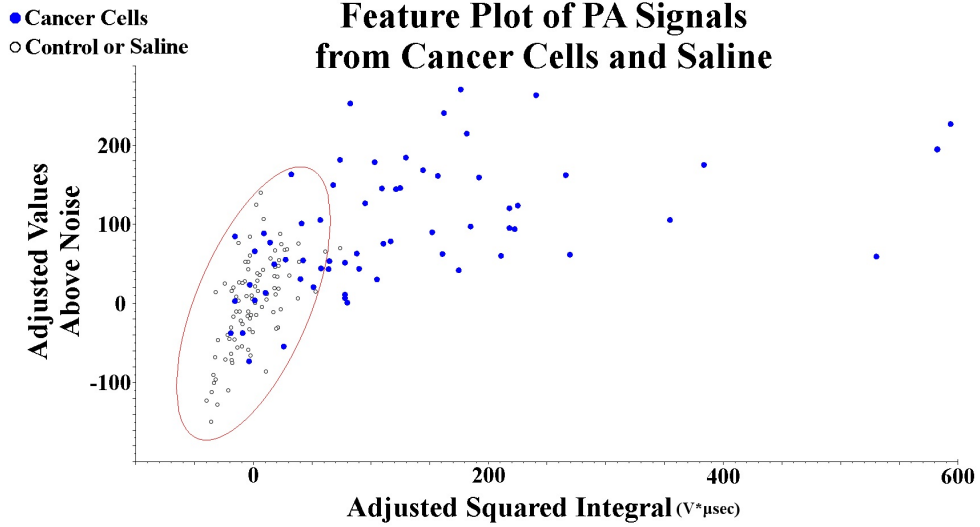


Figure 3.2: A plot of each photoacoustic waveform in two-dimensional feature space from just saline (empty circles, black) and saline with nanoparticle tagged breast cancer cells (full circles, blue) at a concentration of 2 cells/ $3 \mu\text{L}$.

The second feature was a count within the chamber of the number of voltage values which reached above a positive noise threshold or below a negative one. The noise thresholds were determined by a portion of the voltage trace outside of the chamber as the 2.5σ boundaries of the noise. The count of values above or below the noise threshold was adjusted by subtracting from it the count from a portion of the voltage trace outside of the chamber. The basic calculations here are described in Equations 2.2-2.5.

Figure 3.2 is a plot in feature space of each waveform collected from the two groups. There are 92 points in the control or saline group, while there are 64 points in the breast cancer cell group. The red boundary is the 2σ boundary of the control group assuming the distribution is bivariate normal. There is 1 control point outside of the boundary and 42 breast cancer cell points outside of the boundary. This implies that 42 out of 64 signals from the breast cancer sample with 2 cells/ $3 \mu\text{L}$ were significantly different from the PA signals from saline.

The two features computed from the PA waveforms collected from each irradiation measure the presence of large variations from the mean. Both of these time domain features are fairly intuitive since one is an integral and the other a count of values above the noise thresholds (positive and negative). However, frequency domain features and filtering are currently being explored since they may have significant ability to increase signal-to-noise ratio.

The method of classification being used is threshold based since the distribution of features from the saline or control group parameterizes well to a bivariate normal distribution. Other parametric methods were difficult to pursue as the feature distribution from the breast cancer cell group was not easily described by mathematically tractable distributions. Moreover, a threshold based classification method allows for easy control of false-positive and false-negative rates.

The current techniques are adequate as they are able to classify 42 out of 64 signals or 65.6% from a sample with an expected 2 cancer cells/ $3\ \mu\text{L}$. It is important to note that though the expected value is 2 cells/ $3\ \mu\text{L}$ such will not be the case for every occurrence. According to the Poisson distribution, when the expected value is 2, less than or equal to 1 cell has a 40.5% chance of appearing in the laser irradiation. Therefore, 2 or more cells are present 59.5% of the time implying that the current classification rate places the detection limit of the PAFC system somewhere between 1 and 2 cells. This is understandable since the nanoparticle load from one cancer cell to another can vary by up to 2 times or slightly more. Moreover, the position of the cell in the beam spot can also change the sensitivity as the energy profile and acoustic sensitivity are not uniform across the irradiated area or volume. Additionally, there is a 10-20% chance of a breast cancer cell getting 'lost' in the flow system and never making it to the laser irradiation volume.

This detection limit is slightly better than the one reported in the previous chapter.

The improvement may be due to an increase in the amplification used to collect the data. However, it is more likely that this decrease in the detection limit is due to the adjustment of the features with noise within the collected data. By adjusting the features for each acquired waveform they may become invariant to the fluctuations in laser energy during the PAFC test, therefore improving the classification rate. A detection limit of somewhere between 1 and 2 cells is an adequate result to continue with the rest of the test.

3.5 Detection from Normal Blood

A 2 mL volume of blood from a donor was separated into 2 vials with 1 mL each. About 35 cancer cells with DAPI labeled nuclei and tagged with nanoparticles were added to 1 vial. Both vials of blood were centrifuged according to the procedure described in next section. The resulting solutions were tested with the PAFC detection system. The vial without cancer cells was first run through the system as a training set in order to determine the parameters of classification. Following which, the vial with cancer cells was tested under the same parameters. The slugs which tested positive for cancer according to the classification algorithm were captured on a slide. Then a light microscope was used to visualize the cancer cells and withdraw them with a micromanipulator.

3.5.1 Blood Centrifugation Procedure

A 1 mL volume of blood drawn from a healthy individual was layered onto 3 mL of Histopaque 1077 (Sigma Aldrich, St. Louis, MO) in a 15 mL conical cuvette and centrifuged at $400 \times g$ for 30 minutes. After centrifugation, the peripheral mononuclear blood cell (PBMC) layer was withdrawn with a transfer pipette and placed in another

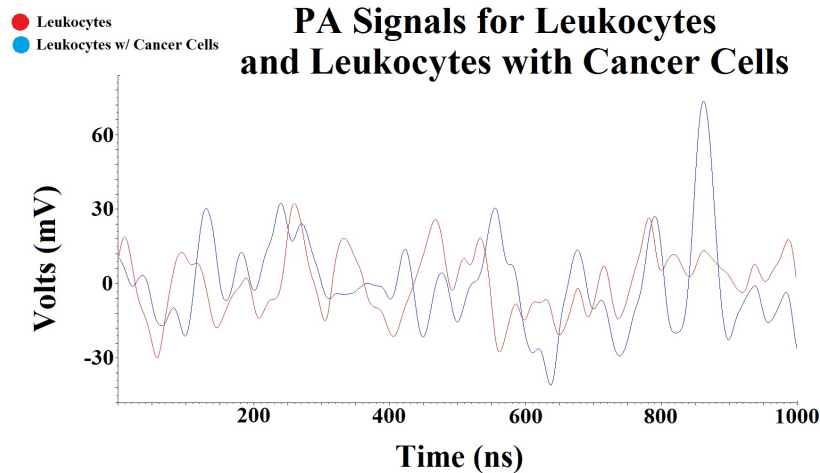


Figure 3.3: (a) Plot of photoacoustic waveforms acquired during the PAFC test from leukocytes with cancer cells. The red trace demonstrates the PA signal when there are no cancer cells but only leukocytes being irradiated in the chamber. The blue trace is the PA signal when there is a cancer cell among the leukocytes.

conical cuvette. The cancer cells in blood are expected to be in the PBMC layer due to their likeness in density with mononuclear leukocytes. This was diluted with 10 mL of 1X PBS and centrifuged at $300 \times g$ for 15 minutes. The supernatant was removed and the cell pellet was resuspended in $500 \mu\text{L}$ of 1X PBS and $500 \mu\text{L}$ of Red Blood Cell Lysis solution (G-Biosciences, St. Louis, MO). This solution was agitated every 2-3 minutes for 10 minutes to aid in lysing the remaining erythrocytes which may cause false positive signals due to hemoglobin pigment. After 10 minutes, this solution was diluted in 2 mL of 1X PBS and centrifuged at $140 \times g$ for 10 minutes. The supernatant was removed and the cell pellet was resuspended in 1 mL of 1X PBS.

In the final part of this study, 1 mL of blood was centrifuged to remove erythrocytes and the remaining leukocytes were resuspended in 1 mL of 1X PBS. About $300 \mu\text{L}$ of this solution was flowed through the system in order to parameterize the PA response of just leukocytes according to the two features used for classification. These parameters were then used for the automated identification of cancer cells

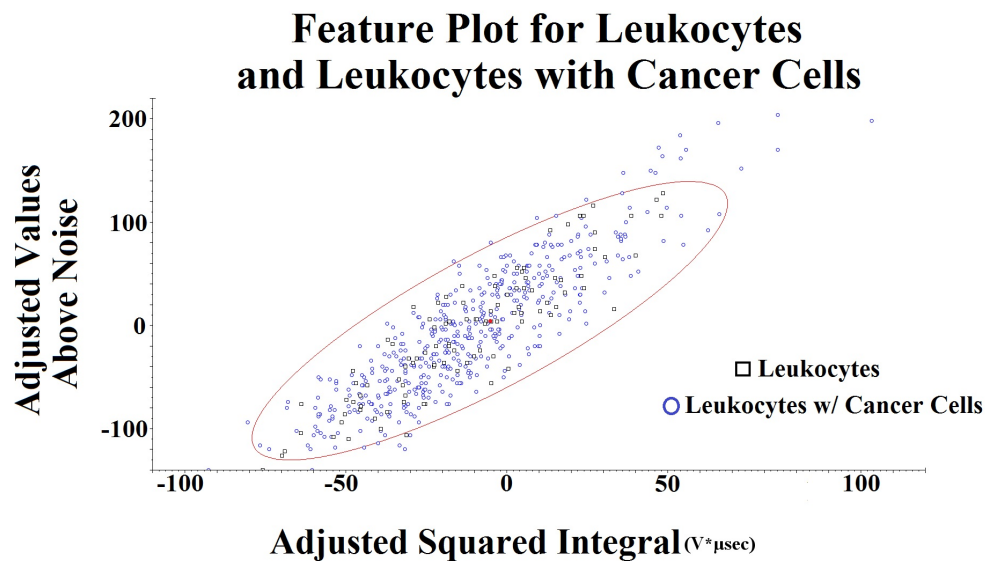


Figure 3.4: A plot of each photoacoustic waveform in two-dimensional feature space from just leukocytes (square) and leukocytes with cancer cells (circle). About 35 cancer cells were added to 1 mL of blood and 17 points appear outside of the boundary and are higher than the mean, which is marked by a full red dot. The outliers towards the bottom-left do not contain PA signals from cancer cells, as their features are much smaller than the mean.

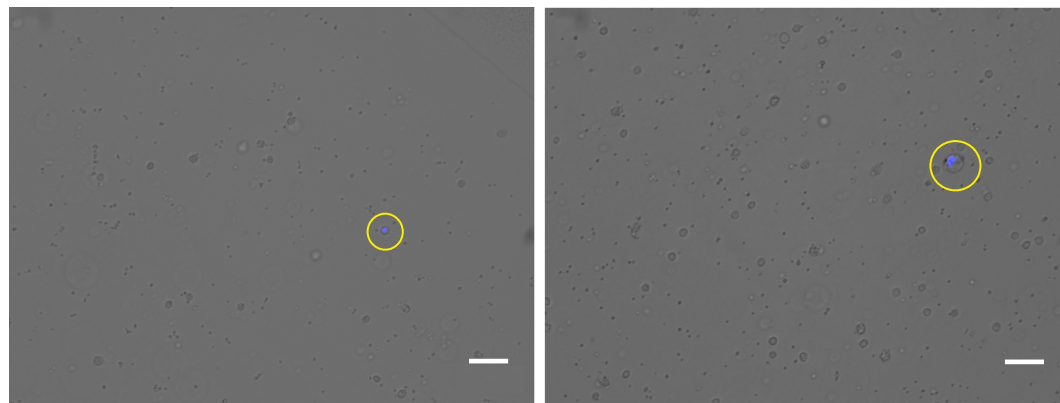


Figure 3.5: Images of 2 out of 15 captured breast cancer cells (circled in yellow) which were retrieved through PAFC detection after approximately 35 cancer cells were added to 1 mL of whole blood. Cancer cells have DAPI labeled nuclei which are blue fluorescent.

among leukocytes, which produce different PA signals with different features. About 35 cancer cells were added to 1 mL of whole blood, the centrifugation procedure was used to remove erythrocytes, the remaining leukocytes and cancer cells were resuspended in 1 mL of 1X PBS. The PAFC system was used to detect and capture the added cancer cells.

3.5.2 Results from the Blood Test

Figure 3.3 demonstrates the PA signals seen by the researchers during the flow tests. The trace in red is characteristic of when there are only leukocytes being irradiated and the blue trace shows the presence of a robust PA emitter between 850-900 ns. Even with cancer cells added, most PA signals resembled the red trace since the presence of a cancer cell in the chamber was an unlikely occurrence due to the small concentration.

This is especially supported by Figure 3.4, which is a feature plot of every PA waveform acquired during the flow test for both samples. The waveforms from the initial sample of just leukocytes are plotted as squares ($n=100$). The red dot at the center of the ellipse is the mean of that distribution and the ellipse is the 2σ boundary. The blue circles ($n=400$) are all of the waveforms acquired during the PAFC test of the second sample which was spiked with cancer cells. Most waveforms are within the red boundary and classified as being not significantly different from just leukocytes. However, outside of the red boundary, towards the top-right, there are 17 outliers which were classified by the automated system as containing cancer cells. These slugs were captured and the isolated cancer cells were imaged. The outliers at the bottom-left were not classified as containing cancer cells because their features were smaller than the mean and the voltage traces did not contain PA signals from cancer cells.

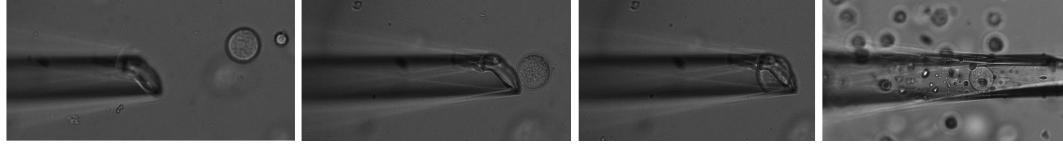


Figure 3.6: Demonstrates how a breast cancer cell is captured out of solution and transported. The cancer cell is within the micropipette in the last image and can be moved to the cap of a PCR tube or a new dish.

3.5.3 Captured Cancer Cells

Figure 3.5a and b are light micrographs of 2 out of 15 total captured cancer cells which were found and imaged. Since the cancer cell nuclei were pre-labeled with DAPI before they were added to the blood, researchers looked for cells with fluorescent blue nuclei. Out of the approximate 35 cancer cells added, 15 were successfully retrieved. Finally, Figure 3.6 demonstrates how a breast cancer cell can be captured and transported with a micromanipulator.

Though 35 cancer cells were added to 1 mL of blood, the initial number of cancer cells added to the blood was probably not exactly 35, since a small volume of stock breast cancer cell suspension was added to the blood. It is safer to assume that the initial number of cancer cells added was within 25-45 cells because the Poisson distribution states that the variance is equal to the expected value when drawing from a large sample.

3.5.4 Discussion of Results

Moreover, the centrifugation procedure used to remove erythrocytes causes 10-30% cell loss for leukocytes and cancer cells (Gertler *et al.*, 2009). This implies that the total number of cancer cells had been reduced to 17-40 cells even before the solution was tested with the PAFC. The automated system classified 17 signals as

being different from leukocytes but only 15 cells were found. This may be because some cells were lost due to the inefficiency of the capturing protocol. For this study, slugs were captured by a human being (fellow lab member) but this procedure is also being automated so as to provide more consistent results. When the system detected a cancer cell, it sounded a loud beep. The slugs which tested positive were captured downstream of where they were irradiated after a specific amount of time, which allowed the slug to reach the end of the chamber.

Since 15 cells were captured and about 35 cells were added, the retrieval rate of the entire protocol with the *in vitro* PAFC is approximately 43%. Nonetheless, it is difficult to determine an exact retrieval rate since there could have been as few as 25 cancer cells added to the blood. If the retrieval rate is indeed 43%, at least 4 cancer cells would have to be present in 1 mL of blood to have about a 90% chance of retrieving 1 cell. Though Guiliano *et al.* (2011) have found with the CellSearch system that 5 cancer cells/7.5 mL of blood has significant prognostic value, Kirby *et al.* (2012) have argued with the GEDI (Geometrically Enhanced Differential Immunocapture) system that CellSearch underestimates the cancer cell concentrations by 2-400 times. From these sources it can be inferred that the *in vitro* PAFC system detects prognostically relevant concentrations of cancer cells in blood.

However, it is important to remember that the cancer cells had been pre-labeled with both DAPI and nanoparticles before they were added to the blood. In a clinical blood test, the cancer cells in the blood cannot be pre-labeled but must be specifically labeled in the presence of leukocytes. As mentioned in Section 4.1, the antibody mediated labeling procedure is currently being optimized since there is some non-specific labeling of leukocytes with nanoparticles. However, once non-specific labeling is reduced, similar retrieval rates are expected since the PAFC is able to detect the presence of 1-2 cancer cells in the chamber.

Figure 3.5 shows images of 2 different captured cancer cells surrounded by leukocytes. The red fluorescence from the fluorescent-gold particle was bleached when the cells were irradiated with the PAFC, making DAPI the only characteristic stain on the cancer cells. Though this method of identification was adequate for this study, a different method of identifying cancer cells will have to be used for a clinically relevant test. The captured breast cancer cells could be labeled with fluorescent antibodies for HER2 (Human Epidermal Growth Factor Receptor 2) or HMFG (Human Milk Fat Globulin) for secondary verification and visual identification.

Finally, Figure 3.6 demonstrates how the identified cell could then be removed from the solution with a micromanipulator controlled micropipette and transported to another location. This new location can be the cap of a PCR tube filled with cell lysis buffer to start the first step to an RT-qPCR method or it could be a petri dish filled with culture media in order to culture this captured cancer cell. Figure 3.7 shows how some cells were transferred to a new slide with 100 μm diameter wells. In a clinical setting, these cells could be fixed and sent to a facility for further molecular characterization.

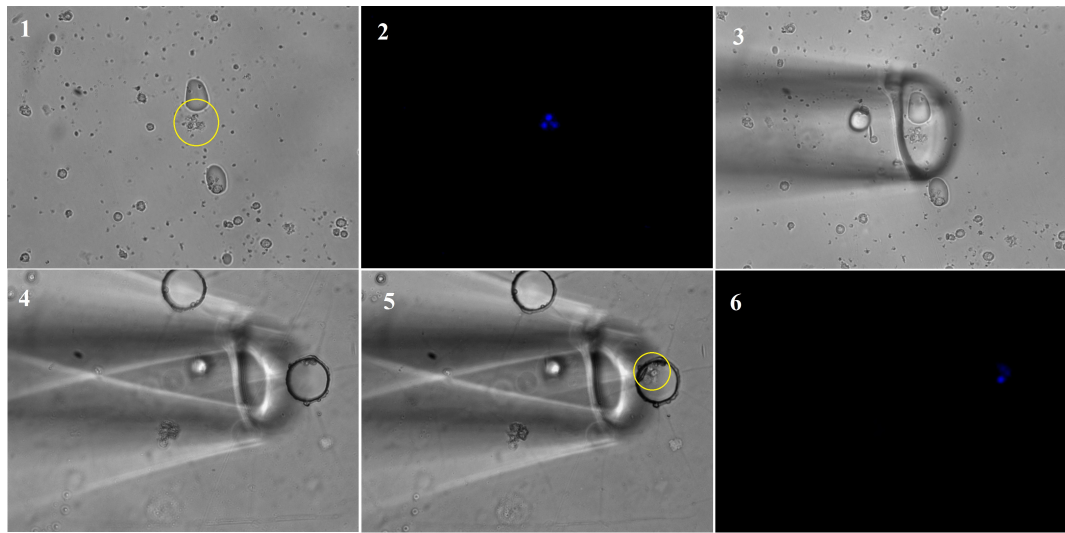


Figure 3.7: A cluster of breast cancer cells is identified through DAPI staining. A micropipette is used to extract the cells and transfer them to a new slide which has 100 micrometer diameter wells. The cells are placed in a well and visualizing the DAPI ensures that they are indeed the same cells as before.

Chapter 4

The Issue of Non-specific Labeling

Any method of detection will have to overcome the issue of background noise. For this to be a viable blood test, breast cancer cells must be targeted with antibody-bound nanoparticles in the presence of leukocytes. Non-specific labeling of leukocytes with these nano-sized photoacoustic contrast agents will create either background noise or false positives during PAFC testing depending on the number of leukocytes which are non-specifically labeled. During this study, the researcher faced multiple issues of non-specific labeling. Those issues are outlined in this chapter.

4.1 EpCAM as the Target

Over expression of EpCAM (epithelial cell adhesion molecule) is characteristic of numerous different cancers (Munz *et al.*, 2009; Went *et al.*, 2006; Armstrong & Eck, 2003; Cimino *et al.*, 2010). Therefore, most receptor-mediated detection and drug therapies for cancer start by targeting the EpCAM cell surface antigen (Osta *et al.*, 2004; Heideman *et al.*, 2001; Olariu *et al.*, 2011). Even other existing circulating tumor cell (CTC) detection platforms use EpCAM as the choice antigen used for cell identification or capture (Nagrath *et al.*, 2007; Riethdorf *et al.*, 2007; Sieuwerts *et al.*, 2009). EpCAM was used in this study to attach nanoparticles to breast cancer cells for all of the previous reasons.

However, using EpCAM as the surface antigen of choice is not without caveats.

One group reports that EpCAM antibodies may bind to LAIR, a leukocyte cell surface receptor, therefore, increasing the occurrence of non-specific binding events (Meyaard *et al.*, 2001). Moreover, multiple groups claim that EpCAM expression may be downregulated in CTCs due to the epithelial mesenchymal transition (EMT) process through which a metastatic cancer cell invades the extracellular matrix (Raimondi *et al.*, 2011; Gorges *et al.*, 2012; van der Gun *et al.*, 2010). On a much more general level, all CTC detection systems are currently calibrated with cultured cancer cell lines and therefore, may not be able to detect circulating tumor cells which are a specific sub-class of all cancer cells. However, these are the current limitations of the technology and must be accepted at face value.

4.2 Non-specific Interactions Without Antibodies

Multiple experiments were carried out with the nanoparticles in suspension with both leukocytes and breast cancer cells in order to quantify non-specific interactions. The cell suspensions used to test the specificity of the nanoparticle label was composed of about 5×10^6 leukocytes derived from blood centrifugation and 5×10^5 T47D breast cancer cells taken from culture in 1 mL of 1 X PBS. In order to distinguish between the two cell types, the breast cancer cell nuclei were labeled with DAPI while the leukocytes were not. Though the concentration of leukocytes is clinically relevant and representative of an actual test, the concentration of breast cancer cells is higher by 10^2 - 10^4 times the clinically relevant number. This discrepancy is necessary so that the results from the nanoparticle labeling could be quantified with fluorescent microscopy since only a small volume ($8 \mu\text{L}$) can be viewed under a slide and both cell types need to be present in the field-of-view.

4.2.1 Non-specific Interaction of Fluorescent Spheres

The natural affinity of the fluorescent spheres and the gold nanoparticles to the breast cancer cells and leukocytes were tested separately. Both breast cancer cells and leukocytes were first incubated with 1 mL of 1% BSA in 1 X PBS for 30 minutes in order to non-specifically block receptor sites on both cell types. This suspension was cleaned by centrifuged at $140\times g$ for 10 minutes and resuspended in 1 mL of 0.1% BSA in 1 X PBS. Then the cells were incubated for 30 minutes with 225×10^6 ($2\ \mu\text{L}$ of stock solution) fluorescent spheres without surface bound antibody or AuNPs. This solution was again centrifuged at $140\times g$ for 10 minutes, the supernatant was removed and the pellet resuspended in 1 mL of 1 X PBS.

Fluorescent imaging of the previous cell sample with Olympus IX70 widefield microscope verified that there was no natural affinity of the fluorescent spheres to either cell type. Over 100 breast cancer cells and leukocytes were tested and none were found to be fluorescent. However, if this same experiment is carried out without the initial step of non-specific receptor blocking with 1% BSA, then some breast cancer cells and leukocytes are randomly labeled with nanoparticles.

4.2.2 Non-specific Interaction of Gold Particles

Apart from determining the non-specific interaction of fluorescent spheres with both cell types, it was also necessary to determine the non-specific interaction of gold particles with both cell types. Breast cancer cells and leukocytes were first incubated with 1 mL of 1% BSA in 1 X PBS for 30 minutes in order to non-specifically block receptor sites on both cell types. This suspension was centrifuged at $140\times g$ for 10 minutes and resuspended in 1 mL of 0.1% BSA in 1 X PBS.

This solution was split in two vials with $500\ \mu\text{L}$ each. The cells in one of the

vials was incubated for 30 minutes with 7.5×10^9 AuNPs ($1.5 \mu\text{L}$ of stock solution) without surface bound antibodies or fluorescent spheres while the other vial was left undisturbed. After 30 minutes, both vials were centrifuged at $140 \times g$ for 10 minutes. After discarding the supernatant, the cell pellet from each vial was removed and tested with the setup demonstrated in Figure 2.1. Both samples were irradiated with the previously described laser with one pulse at 532 nm with $100\text{-}125 \text{ mJ/cm}^2$ in a 5 ns pulse. The photoacoustic signals from both samples were normalized with the radiant exposure and compared to determine presence of AuNPs.

This procedure was repeated five times for five different samples and a Student's T-test did not find a significant difference between the photoacoustic signals from the two samples indicating the AuNPs did not non-specifically interact with the 1% BSA blocked breast cancer cell or leukocyte. This experiment was not repeated without BSA blocking. However, it is likely that if BSA was not used first, then the AuNPs would have non-specifically attached to both cell types.

4.3 Binding of Fluorescent-Gold anti-EpCAM Conjugate to Cells

A similar cell suspension as the one described in Section 4.2 was used to test the specificity of the antibody nanoparticle conjugate to both breast cancer cells and leukocytes. The cell suspension, without any blocking, was incubated in 1 mL of 0.1% BSA with $80 \mu\text{L}$ of the nanoparticle antibody conjugate (described in Section 2.1.2) to determine both specific and non-specific interaction. After 30 minutes, the cells were cleaned through centrifugation at $140 \times g$ and resuspended in 1 X PBS. Figure 4.1 demonstrates the difference between the labeling of breast cancer cells as opposed to leukocytes.

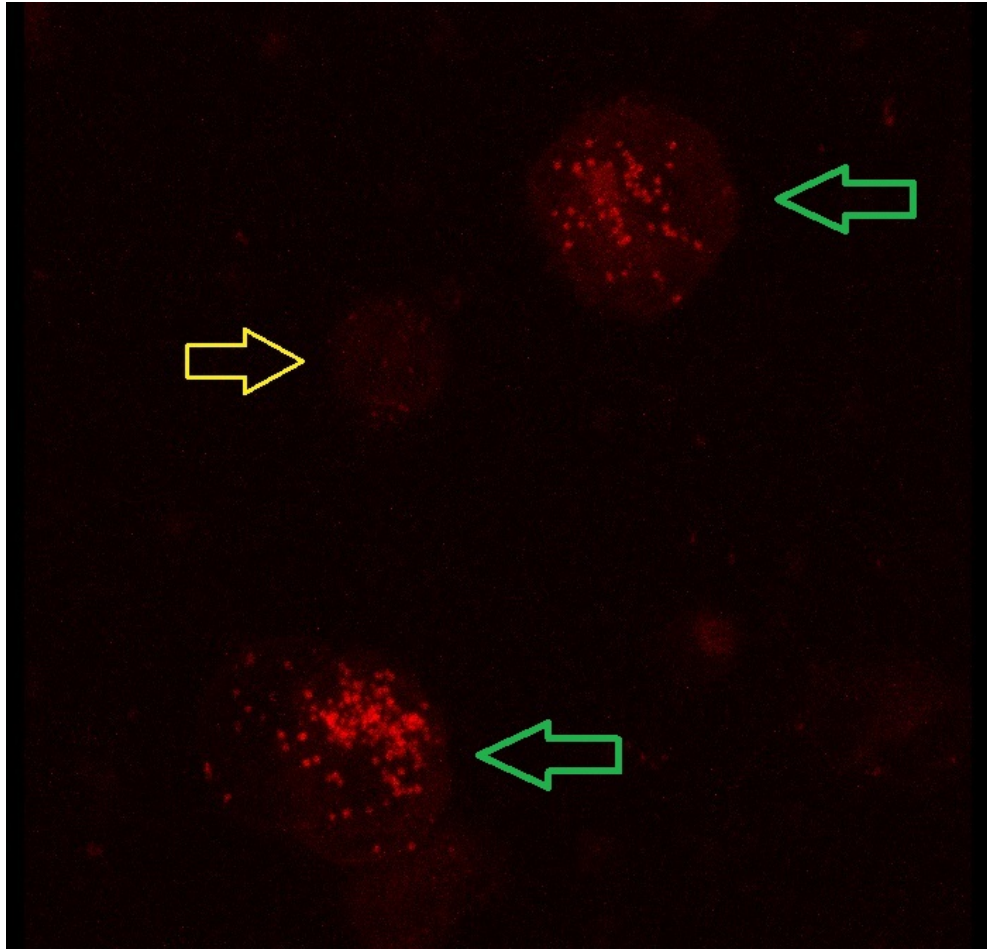


Figure 4.1: This image demonstrates the un-intended labeling of leukocytes with fluorescent-gold nanoparticles developed in this study. The two green arrows pointing to the left indicate two breast cancer cells. While the one yellow arrow pointing to the right, indicates a single leukocyte which is labeled. About 5% of leukocytes are labeled, each with one-tenth to one-fifth as many nanoparticles as found on a single breast cancer cell.

While all of the breast cancer cells were labeled about equally with the antibody conjugated nanoparticles, only about 5% of the leukocytes were labeled with about $\frac{1}{10}$ - $\frac{1}{5}$ as many nanoparticles as found on the average cancer cell. This demonstrates that even without a blocking buffer, the nanoparticle-antibody conjugate was fairly specific to the breast cancer cells in the presence of leukocytes.

In a different set of experiments, the cell suspension of leukocytes and cancer cells were incubated for 30 minutes in 1 mL of 1% BSA and 5% mouse serum in 1 X PBS. Mouse serum was present in this blocking buffer since the anti-EpCAM antibodies used in this study were grown in mouse and targeted to human. The cells were then centrifuged out of this suspension and resuspended in a 0.1% BSA and 0.1% mouse serum and 80 μ L of the nanoparticle antibody conjugate for 30 minutes.

Through fluorescent imaging it was determined that there was a $18\pm 2\%$ decrease in breast cancer cell labeling and a $50\pm 3\%$ decrease in leukocyte labeling when a blocking buffer was used. Moreover, a smaller proportion of leukocytes, about 3%, were labeled with nanoparticles. Increasing the concentration of mouse serum to 10% in the blocking buffer did not change this result significantly.

4.4 Implications of Non-specific Labeling

Currently, during the PAFC test, the leukocytes and cancer cells retrieved from 1 mL of blood are resuspended in 1 mL of 1 X PBS and tested with the system. In this case, the breast cancer cells had been labeled before being added to the whole blood. However, in the actual clinical scenario, the label will have to be introduced to the cancer cells while they are in suspension with the leukocytes after both have been separated from the erythrocytes through centrifugation. Therefore, some leukocytes will be non-specifically labeled.

The biological relevant concentrations of CTCs is expected to be 0-1000 cells/mL of normal blood (Giuliano *et al.*, 2011; Kirby *et al.*, 2012). It is well accepted that the number of leukocytes ranges from $5-10 \times 10^6$ /mL of normal blood. If we assume that after the blood centrifugation protocol 10-30% of leukocytes are lost, then about 6×10^6 leukocytes will be retrieved (Gertler *et al.*, 2009). If the nanoparticle labeling is carried out with blocking buffers, then 3% or 1.8×10^5 cells will be labeled.

Each time the laser fires in the PAFC, $3 \mu\text{L}$ of the suspension is irradiated. This means that about 540 out of the 1.8×10^5 non-specifically labeled cells will be irradiated with each pulse. Since the blocking buffer reduces the labeling by 50%, each of these leukocytes will have $\frac{1}{20} - \frac{1}{10}$ the number of nanoparticles on the average cancer cell. This implies that there will be about 40 photoacoustic emitters 'equivalent' to breast cancer cells in the chamber at all times as the background noise. This makes it nearly impossible to detect the presence of one cancer cell.

If the non-specific labeling can be reduced by 4 times, either by reducing the number of labeled cells or the amount of nanoparticles on the cells, then it would reduce the number of equivalent emitters to 10 and make it possible to detect one cancer cell. This may not be possible to do by targeting EpCAM and new surface antigens need to be explored to identify one which will work. This is further elaborated on in the following section.

Additionally, there are some protocol changes which may be able to work around the non-specific labeling issue. One could dilute the sample in 4 times as much PBS and effectively reduce the number of equivalent emitters in the chamber. However, this would increase the testing time by 4 times as well (from 30 minutes to 2 hours). The testing volume could also be decreased by 4 times if the chamber diameter is reduced by 2 fold. The increase in testing time could be compensated for by an increase in the repetition rate of the laser. For instance, if the laser was used at 80 Hz

instead of 20 Hz as it is used now, then the background signals could be reduced by using larger dilution volumes and still retain the current testing time.

It may be beneficial to develop a simulation of spherical photoacoustic emitters with different intensities. This would provide a more mathematically rigorous support for the threshold of background emitters at which the PA signal from a single cancer cell in the presence of leukocytes can be distinguished.

4.5 Further Research on Target Antigens

Apart from changing the parameters of the system, the surface antigen targeted on the breast cancer cell can also be changed in order to reduce non-specific labeling. The following surface antigens have also found to be over-expressed in breast cancer cells (Boire *et al.*, 2005; Baselga *et al.*, 1997; Rakha *et al.*, 2005; Surmacz, 2000):

- (1) PAR1 – protease activated receptor 1
- (2) HER2 – human epidermal growth factor receptor 2
- (3) MUC1 and MUC4 – mucin 1 and mucin 4
- (4) IGF-IR – insulin like growth factor I receptor

To test the specificity of the antibodies of these receptors to the breast cancer cells, it is best to follow a similar protocol as described above. FITC conjugated antibodies to these specific receptors are available through Pierce Antibodies. Breast cancer cells and leukocytes could be labeled separately and tested with FACS in order to get large samples and determine with mathematical accuracy the difference in labeling of the two cell types. If the non-specific labeling is reduced by at least 4 times when compared to the findings with anti-EpCAM, a potential target antigen is found. This reduction can either be a reduction in the proportion of leukocytes which are non-specifically labeled or a reduction in the amount of relative label on the leukocytes

when compared to the cancer cells.

It may be that none of these potential surface antigen targets allow for the kind of reduction in non-specific labeling that is necessary to improve the system. If that is the case, the best one will have to be picked and implemented in combination with the changes suggested for the parameters of the test e.g. dilution volume and laser repetition rate.

Chapter 5

Summary and Concluding Remarks

A dual modality nanoparticle, which is both a strong fluorescent and photoacoustic emitter, is attached to breast cancer cells using anti-EpCAM. Certain features are identified in the photoacoustic signal during a flow cytometry test which can be used for automated classification of cancer cells. Additional metrics in the frequency domain can be added to the two existing ones defined by Equations 2.1 and 2.5. These new metrics can be the power at some frequency or the ratio of powers at different frequencies from the photoacoustic signal. A method was developed to analyze the feature space and determine threshold boundaries which would be used to classify certain 'slugs' as containing a PA signal from a cancer cell.

The additional work in this study demonstrates that if a breast cancer cell can be labeled specifically then about 40% of the breast cancer cells in a blood sample can be detected and retrieved through the PAFC system. A protocol is established and an automated photoacoustic flow cytometer was programmed with classification algorithms and used to capture cells during the flow test. Finally, the issue of non-specific labeling is covered in some depth and a protocol is proposed to combat it and the problems which arise from it.

As it stands now, the work is incomplete since it cannot be directly translated to patient blood. The PAFC is currently changing by reducing the diameter of the flow chamber to $400\ \mu\text{m}$ and increasing the laser repetition rate to 50 Hz. These changes to the parameters may be adequate in combating the background noise from the

non-specifically labeled leukocytes. It reduces the detection volume by more than 9 times and the number of equivalent emitters to less than 5. More tests will be needed under this modified flow system to determine if it does indeed trivialize the non-specific labeling issue.

Additionally, it is suggested that new surface antigen targets are identified through the protocol described in Section 4.5. This will likely be a longer process but will help identify the optimal antigen target to be used for this technique.

If these proposed methods reduce non-specific labeling, then it will be relatively simple to reproduce this work done on pre-labeled breast cancer cells which were spiked into whole blood. At that time, the contents of this document should provide the right amount of guidance to finish this project and extend photoacoustic flow cytometry to non-pigmented cancers in a clinically relevant way.

Appendix A

Calculations for Antibody-Nanoparticle Conjugation

A fluorescent-gold nanoparticle conjugate was made for the purposes of adding photoacoustic contrast to the breast cancer cells. This was done by conjugating a 300 nm red-fluorescent (TRITC) microsphere to 54 nm spherical gold particles. The gold particles provided the photoacoustic contrast while the fluorescent microsphere allowed the researchers to visualize and verify nanoparticle attachment to the cancer cell under light microscopy. Traditionally, electron microscopy would be necessary to visualize metallic particles, but by pairing the gold nanoparticles with the fluorescent latex spheres, particle attachment could be verified easily by light microscopy.

Figure A.1 demonstrates how the fluorescent and gold nanoparticles were conjugated. Biotinylated anti-EpCAM was bound to 300 nm fluorescent bead first. Then the remaining biotin on the anti-EpCAM was used to bind the gold particle. Finally, the whole nanoparticle compound was coated in a layer of biotinylated anti-EpCAM by using the remaining streptavidin on the AuNP and fluorescent bead. Most of the existing protocols to make such nanoparticle-nanoparticle or antibody-nanoparticle conjugates seemed arbitrary in their directions. I have arrived at the protocol reported

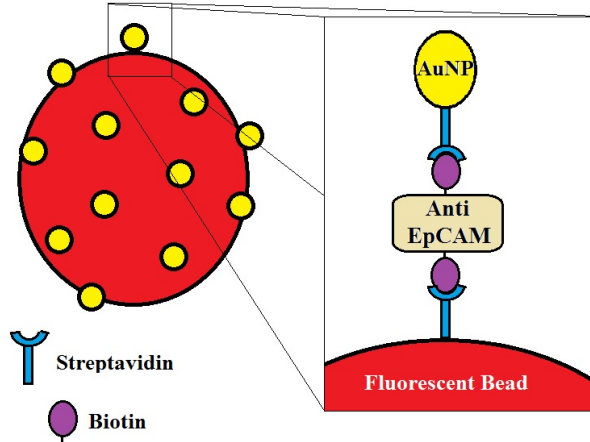


Figure A.1: A schematic of how the fluorescent gold nanoparticle conjugate was made. Biotinylated anti-EpCAM was bound to 300 nm fluorescent bead first. Then the remaining biotin on the anti-EpCAM was used to bind the gold particle. Please note that figure is not to scale.

in Section 2.1.2 through the following calculations.

The biotinylated anti-EpCAM has a molecular mass of 40 kDa as indicated by Pierce Antibodies, from where the anti-EpCAM was purchased. From this molecular mass, a density of 1.36 g/cm^3 can be inferred due to the work of Fischer *et al.* (2009). By using Avagadro's number, one can calculate that the mass of one molecule of anti-EpCAM is approximately $6.6 \times 10^{-20} \text{ g}$. If the molecule is assumed to be a perfect sphere, then it would have a radius of 2.2 nm as calculated from the density. The surface area of the red-flourescent particle is about $3.2 \times 10^5 \text{ nm}^2$ and the cross-sectional area of a single protein molecule would be 15.2 nm^2 . If we allow about 45 nm as the mean distance between protein molecules bound to the red-flourescent particle, there would 163 anti-EpCAM molecules per red-flourescent sphere. The mean distance of 45 nm is justified by the fact that the anti-EpCAM molecules will be used to bind gold nanoparticles to the fluorescent bead. Since the AuNPs have a diameter of about 50 nm, the distance from the center of one AuNP to another would have to

be 50 nm. This implies that on the surface of the sphere, the anti-EpCAM molecules should be about 45 nm apart so as to ensure that the smallest amount of antibodies are used per trial due to their cost.

From the original concentration of $200 \mu\text{g}/\text{mL}$ for the anti-EpCAM stock solution, one can calculate that it implies a molecular concentration of 3×10^{15} protein molecules/mL. Additionally, the concentration of the red-fluorescent microspheres is reported by Bangs Labs, the supplier, to be 500×10^9 . Using these concentrations and the ratio of 1:163 of red-fluorescent spheres to anti-EpCAM molecules, one can come up with any number of combinations which will work.

However, it is also important to dilute the number of fluorescent spheres and anti-EpCAM molecules into an appropriate volume so as to reduce clumping of fluorescent spheres by binding to the same protein molecule. This optimal concentration would depend upon the diffusion coefficient of both materials and the characteristic time constant of the reaction. Such data are unknown so it is difficult to give the protocol used in this study a firm mathematical grounding. The researcher, therefore, reacted the red-fluorescent beads in such a suspension that the mean free path between two fluorescent beads was more than 10 times the diameter of the beads. Since the fluorescent beads have a diameter of about 300 nm, they would have to be in a dilution of about 225×10^8 beads/mL to keep a mean free path of about $3.5 \mu\text{m}$. The correct amount of anti-EpCAM was added to this solution and allowed to react for 30 minutes, which is enough time to allow for diffusion to take place.

A.1 AuNPs to Anti-EpCAM on Fluorescent Bead

To this solution, gold nanoparticles were then added in order to bind the AuNPs to the fluorescent beads with the anti-EpCAM. One can easily calculate that at

most approximately 120 gold nanoparticles, 50 nm in diameter can fit on the 300 nm fluorescent bead. It is likely that less than half this many would successfully bind to a fluorescent bead since access to the surface of the fluorescent bead would be impeded as more gold nanoparticles attached. If the mean free distance between two gold nanoparticles on the surface of a fluorescent bead was taken to 100 nm, then approximately 14 AuNPs would fit on the surface of a fluorescent bead. This ratio can be used to determine the appropriate number of AuNPs needed to cover the fluorescent bead.

Barring all of these calculations, clusters of particles still form as the suspension is centrifuged to clean of excess anti-EpCAM and gold nanoparticles which do not precipitate when centrifuged at $550\times g$ for 8 minutes. When centrifuged, the conjugated AuNPs form a pellet and the rest of the reactions can be carried out in this pellet. Clusters can form when all of the nanoparticles are hyper-concentrated in this pellet form. Though this may seem disadvantageous, it actually works to the researchers benefit, as the conjugated nanoparticles become stable and generally don't react with one another beyond this point.

A.2 Nanoparticle Conjugate Storage

A suspension of nanoparticles like this must be stored in 0.1% BSA in 1XPBS for 2 weeks, beyond which the age of the nanoparticle conjugate starts to affect experimental results. These considerations can be used as a guide to the right proportions of reactants. However, some empirical testing may also be required in order to find the optimal concentrations.

BIBLIOGRAPHY

Acharya, S., Dilnawaz, F., & Sahoo, S.K. 2009. Targeted epidermal growth factor receptor nanoparticle bioconjugates for breast cancer therapy. *Biomaterials*, **30**, 5737–5750.

ACS. 2013. *Breast Cancer*. American Cancer Society <http://www.cancer.org/acs/groups/cid/documents/webcontent/003090-pdf.pdf>.

Agarwal, A., Huang, S.W., ODonnell, M., Day, K.C., Day, M., Kotov, N., & Ashkenazi, S. 2007. Targeted gold nanorod contrast agent for prostate cancer detection by photoacoustic imaging. *Journal of Applied Physics*, **102**, 064701.

Armstrong, A., & Eck, S.L. 2003. EpCAM: a new therapeutic target for an old cancer antigen. *Cancer Biology and Therapy*, **2**, 320–326.

Baselga, J., Seidman, A.D., Rosen, P.P., & Norton, L. 1997. HER2 overexpression and paclitaxel sensitivity in breast cancer: therapeutic implications. *Oncology-Huntington*, **11**, 43.

Boire, A., Covic, L., Agarwal, A., Jacques, S., Sherifi, S., & Kuliopulos, A. 2005. PAR1 is a matrix metalloprotease-1 receptor that promotes invasion and tumorigenesis of breast cancer cells. *Cell*, **120**, 303–313.

Cimino, A., Halushka, M., Illei, P., Sukumaran, X. Wuand S., & Argani, P. 2010. Epithelial cell adhesion molecule (EpCAM) is overexpressed in breast cancer metastases. *Breast Cancer Research and Treatment*, **123**, 701–708.

Cross, S.E., Jin, Y.S., Jianyu, R., & Gimzewski, J.K. 2007. Nanomechanical analysis of cells from cancer patients. *Nature Nanotechnology*, **12**, 780–783.

- Daniel, M.C., & Astruc, D. 2004. Gold nanoparticles: assembly, supramolecular chemistry, quantum-size-related properties, and applications toward biology, catalysis, and nanotechnology. *Nature Biotechnology*, **104**, 293.
- de Broek, B. Van, Devoogdt, N., Hollander, D.A., Gijs, H.L., Jans, K., Lagae, L., Muyledermas, S., Maes, G., & Borghs, G. 2011. Specific cell targeting with nanobody conjugated branched gold nanoparticles for photothermal therapy. *ACS Nano*, **5**, 4319–4328.
- Dick, J.E. 2003. Breast cancer stem cells revealed. *PNAS*, **100**, 3547–3549.
- Dumitras, D.C., Dutu, D.C., Matei, C., Magureanu, A.M., Petrus, M., & Popa, C. 2007. Laser photoacoustic spectroscopy: principles, instrumentation, and characterization. *Journal of Optoelectronics and Advanced Materials*, **9**, 3655–3701.
- Fillmore, C.M., & Kuperwasser, C. 2008. Human breast cancer cell lines contain stem-like cells that self-renew, give rise to phenotypically diverse progeny and survive chemotherapy. *Breast Cancer Research*, **10**, 10.1186/bcr1982.
- Fischer, H., Polikarpov, I., & Craievich, A.F. 2009. Average protein density is a molecular weight dependent function. *Protein Science*, **10**, 2825–2828.
- Furman-Haran, E., Grobgeld, D., Kelcz, F., & Degani, H. 2001. Critical role of spatial resolution in contrast enhanced breast MRI. *Journal of Magnetic Resonance Imaging*, **13**, 862–867.
- Gertler, R., Rosenberg, R., Fuehrer, K., Dahm, M., Nekarda, H., & Siewert, J.R. 2009. Detection of circulating tumor cells in blood using an optimized density gradient centrifugation. *Recent Results in Cancer Research*, **162**, 149–155.

- Giuliano, M., Giordano, A., Jackson, S., Hess, K.R., Giorgi, U. De, Mego, M., Handy, B.C., Ueno, N.T., Alvarez, R.H., Laurentiis, M.D., Placido, S.D., Valero, V., Hortobagyi, G.N., Reuben, J.M., & Cristofanilli, M. 2011. Circulating tumor cells as prognostic and predictive markers in metastatic breast cancer patients receiving first-line systemic treatment. *Breast Cancer Research*, **13**, R67.
- Givan, A.L. 2001. Principles of Flow Cytometry: An Overview. *Methods in Cell Biology*, **63**, 19–50.
- Gorges, T., Tinhofer, I., Drosch, M., Rose, L., Zollner, T., Krahn, T., & von Ahsen, O. 2012. Circulating tumour cells escape from EpCAM-based detection due to epithelial-to-mesenchymal transition. *BMC Cancer*, **12**, 178.
- Gupta, P.G., & Massague, J. 2006. Cancer metastasis: building a framework. *Cell*, **127**, 679–695.
- Gutierrez-Juarez, G., Gupta, S.K., Al-Shaer, M., Polo-Parada, L., Dale, P.S., Papanagorgio, C., & Viator, J.A. 2010. Detection of melanoma cells in vitro using an optical detector of photoacoustic waves. *Lasers in Surgery and Medicine*, **42**, 274–281.
- Hazan, R.B., Phillips, G.R., Qiao, R.F., Norton, L., & Aaronson, S.A. 2000. Exogenous expression of N-cadherin in breast cancer cells induces cell migration, invasion, and metastasis. *Journal of Cell Biology*, **148**, 779–790.
- Heideman, D.A.M., Snijders, P.J.F., Craanen, M.E., Bloemena, E., Meijer, C.J.L.M., Meuwissen, S.G.M., van Beusechem, V.W., Pinedo, H.M., Curiel, D.T., Hiasma, H.J., & Gerritsen, W.R. 2001. Selective gene delivery toward gastric and esophageal adenocarcinoma cells via EpCAM-targeted adenoviral vectors. *Cancer Gene Therapy*, **8**, 342–351.

- Hinton, C.V., Avraham, S., & Avraham, H.K. 2010. Role of CXCR4/CXCL12 signaling axis in breast cancer metastasis to brain. *Clinical and Experimental Metastasis*, **27**, 97–105.
- Huynh, P.T., Jarolimek, A.M., & Daye, S. 1998. The false negative mammogram. *Radiographics*, **18**, 1137–1154.
- Kang, B., Yu, D., Dai, Y., Chang, S., Chen, D., & Ding, Y. 2009. Cancer Cell Targeting and Photoacoustic Therapy Using Carbon Nanotubes as Bomb Agents. *Small*, **25**, 1292–1301.
- Kirby, B.J., Jodari, M., Loftus, M.S., Gakhar, G., Pratt, E.D., Chanel-Vos, C., Gleghorn, J.P., Santana, S.M., Liu, H., Smith, J.P., Navarro, V., Tagawa, S.T., Bander, N.H., Nanus, D.M., & Giannakakou, P. 2012. Functional Characterization of Circulating Tumor Cells with a Prostate-Cancer-Specific Microfluidic Device. *PLoS ONE*, **7**, e35976.
- Mallidi, S., Luke, G.P., & Emelianov, S. 2011. Photoacoustic imaging in cancer detection, diagnosis, and treatment guidance. *Trends in Biotechnology*, **29**, 213–221.
- Maslov, K., Zhang, H.F., Hu, S., & Wang, L.V. 2008. Optical-resolution photoacoustic microscopy for in vivo imaging of single capillaries. *Optics Letters*, **33**, 929–931.
- McCormack, D., Al-Shaer, M., Goldschmidt, B.S., Dale, P.S., Papageorgio, H.C., Bhattacharyya, K., & Viator, J.A. 2009. Photoacoustic Detection of Melanoma Micrometastasis in Sentinel Lymph Nodes. *Journal of Biomechanical Engineering*, **131**, 074519.
- McCormack, D.R., Bhattacharyya, K., Kannan, R., Katti, K., & Viator, J.A. 2011.

Enhanced photoacoustic detection of melanoma cells using gold nanoparticles. *Lasers in Surgery and Medicine*, **43**, 333–338.

McKinnel, R.G., Parchment, R.E., Perantoni, A.O., Damjanov, I., & Pierce, G.B. 2006. *The biological basis of cancer*. Second edn. New York, NY, USA: Cambridge University Press.

Meyaard, L., de Ruiter, T., Lanier, L.L., Phillips, J.H., & Clevers, H. 2001. The epithelial cellular adhesion molecule (Ep-CAM) is a ligand for the leukocyte-associated immunoglobulin-like receptor (LAIR). *Journal of Experimental Medicine*, **194**, 107–112.

Munz, M., Baeuerle, P.A., & Gires, O. 2009. The emerging role of EpCAM in cancer and stem cell signaling. *Cancer research*, **69**, 5627–5629.

Nagrath, S., Sequist, L.V., Maheswaran, S., Bell, D.W., Irimia, D., Ulkus, L., Smith, M.R., Kwak, E.L., Diggumarthi, S., Muzikansky, A., Ryan, P., Ballis, U.J., Tompkins, R.G., Haber, D.A., & Toner, M. 2007. Isolation of rare circulating tumour cells in cancer patients by microchip technology. *Nature*, **450**, 1235–1239.

O'Brien, C.M., Rood, K.D., Bhattacharyya, K., DeSouza, T., Sengupta, S., Gupta, S.K., Mosley, J.D., Goldschmidt, B.S., Sharma, N., & Viator, J.A. 2012. Capture of circulating tumor cells using photoacoustic flowmetry and two phase flow. *Journal of Biomedical Optics*, **17**, 061221.

Olariu, C.I., Yiu, H.H.P., Bouffier, L., Nedjadi, T., Costello, E., Williams, S.R., Halloran, C.M., & Rosseinsky, M.J. 2011. Multifunctional Fe₃O₄ nanoparticles for targeted bi-modal imaging of pancreatic cancer. *Journal of Materials Chemistry*, **21**, 12650–12659.

- Oraevsky, A.A., Karabutov, A.A., & Savateeva, E.V. 2001. Enhancement of optoacoustic tissue contrast with absorbing nanoparticles. *European Conference on Biomedical Optics, International Society for Optics and Photonics*, 60–69.
- Osta, W.A., Chen, Y., Mikhitarian, K., Mitas, M., Salem, M., Hannun, Y.A., Cole, D.J., & Gillanders, W.E. 2004. EpCAM is overexpressed in breast cancer and is a potential target for breast cancer gene therapy. *Cancer Research*, **64**, 5818–5824.
- Paltauf, G., & Schmidt-Kloiber, H. 1997. Measurement of laser-induced acoustic waves with a calibrated optical transducer. *Journal of Applied Physics*, **82**, 1525–1531.
- Paterlini-Berchot, P., & Benali, N.L. 2007. Circulating tumor cells (CTC) detection: clinical impact and future directions. *Cancer Letters*, **253**, 180–204.
- Raimondi, C., Gradilone, A., Naso, G., Vincenzi, B., Petracca, A., Nicolazzo, C., Saltirelli, A. Palazzo R., Spremberg, F., Cortesi, E., & Gazzaniga, P. 2011. Epithelial-mesenchymal transition and stemness features in circulating tumor cells from breast cancer patients. *Breast Cancer Research and Treatment*, **130**, 449–455.
- Rakha, E.A., Boyce, R.W.G., El-Rehim, D.A., Kurien, T., Green, A.R., Paish, E.C., Robertson, J.F.R., & Ellis, I.O. 2005. Expression of mucins (MUC1, MUC2, MUC3, MUC4, MUC5AC and MUC6) and their prognostic significance in human breast cancer. *Modern Pathology*, **18**, 1295–1304.
- Ramaswamy, S., Ross, K.N., Lander, E.S., & Golub, T.R. 2002. A molecular signature of metastasis in primary solid tumors. *Nature Genetics*, **33**, 49–54.
- Riethdorf, S., Fritsche, H., Muller, V., Rau, T., Schindlbeck, C., Rack, B., Janni, W., Coith, C., Beck, K., Janicke, F., Jackson, S., Gornet, T., Cristofanilli, M., &

- Pantel, K. 2007. Detection of circulating tumor cells in peripheral blood of patients with metastatic breast cancer: a validation study of the CellSearch system. *Clinical Cancer Research*, **13**, 920–928.
- Rooth, R.A., Verhage, A.J.L., & Wouters, L.W. 1990. Photoacoustic measurement of ammonia in the atmosphere: influence of water vapor and carbon dioxide. *Applied Optics*, **29**, 3643–3653.
- Rosencwaig, A., & Gersho, A. 1976. Theory of photoacoustic effect with solids. *Journal of Applied Physics*, **47**, 64–69.
- Sethuraman, S., Amirian, J.H., Litovsky, S.H., Smalling, R.W., & Emelianov, S.Y. 2008. Spectroscopic intravascular photoacoustic imaging to differentiate atherosclerotic plaques. *Optics Express*, **16**, 3362–3367.
- Sieuwert, A.M., Kraan, J., Bolt, J., Spoel, P.V.D., Elstrodt, F., Schutte, M., Martens, J.M.W., Gratama, J.W., Sleijfer, S., & Foekens, J.A. 2009. Anti-epithelial cell adhesion molecule antibodies and the detection of circulating normal-like breast tumor cells. *Journal of the National Cancer Institute*, **10**, 61–66.
- Sloan, E.K., & Anderson, R.L. 2002. Genes involved in breast cancer metastasis to bone. *Cellular and Molecular Life Sciences*, **59**, 1491–1502.
- Suemune, I., Yamamoto, H., & Yamanishi, M. 1985. Surface and subsurface structure of solids by laser photoacoustic spectroscopy. *Journal of Applied Physics*, **58**, 615–617.
- Surmacz, E. 2000. Function of the IGF-I receptor in breast cancer. *Journal of Mammary Gland Biology and Neoplasia*, **5**, 95–105.
- Takao, M., & Takeda, K. 2010. Enumeration, Characterization, and Collection of

Intact Circulating Tumor Cells by Cross-Contamination Free Flow Cytometry. *Cytometry Part A*, **79**, 107–117.

van de Vijver, M.J., He, Y.D., vant de Veer, L.J., Dai, H., Hart, A.A.M., Voskuil, D.M., Schreiber, G.J., Peterese, J.L., Roberts, C., Martin, M.J., Parrish, M., Atsma, D., Witteween, A., Glas, A., Delahaye, L., van der Velde, T., Bartelink, H., Rodenhuis, H., Rutgers, E.T., Friend, S.H., & Bernards, R. 2002. A gene-expression signature as a predictor of survival in breast cancer. *New England Journal of Medicine*, **347**, 1999–2009.

van der Gun, B.T.F, Melchers, L.J., Ruiters, M.H.J., de Leij, L.F.M.H., McLaughlin, P.M.J., & Rots, M.G. 2010. EpCAM in carcinogenesis: the good, the bad or the ugly. *Carcinogenesis*, **31**, 1913–1921.

Viator, J.A., Au, G., Paltauf, G., Jacques, S.L., Prahl, S.A., Ren, H., Chen, Z., & Nelson, J.S. 2002. Clinical testing of a photoacoustic probe for port wine stain depth determination. *Lasers in Surgery and Medicine*, **30**, 141–148.

Viator, J.A., Komadina, J., Svaasand, L.O., Aguilar, G., Choi, B., & Nelson, J.S. 2004. A comparative study of photoacoustic and reflectance methods for determination of epidermal melanin content. *Journal of Investigative Dermatology*, **122**, 1432–1439.

Viator, J.A., Gupta, S., Goldschmidt, B.S., Bhattacharyya, K., Kannan, R., Shukla, R., Dale, P.S., Boote, E., & Katti, K. 2010. Gold nanoparticle mediated detection of prostate cancer cells using photoacoustic flowmetry with optical reflectance. *Journal of Biomedical Nanotechnology*, **6**, 187–191.

Wang, M., & Thanou, M. 2010. Targeting nanoparticles to cancer. *Pharmacological Research*, **62**, 90–99.

- Weigelt, B., Peterese, J.L., & vant Veer, L.J. 2005. Breast cancer metastasis: markers and models. *Nature Reviews: Cancer*, **5**, 591–602.
- Weight, R.M., Viator, J.A., Dale, P.S., Caldwell, C.W., & Lisle, A.E. 2006. Photoacoustic detection of metastatic melanoma cells in the human circulatory system. *Optics Letters*, **31**, 2998–3000.
- Went, P., Vasei, M., Bubendorf, L., Terracciano, L., Tornillo, L., Riede, U., Kononen, J., Simon, R., Sauter, G., & Baeuerle, P. A. 2006. Frequent high-level expression of the immunotherapeutic target Ep-CAM in colon, stomach, prostate and lung cancers. *British Journal of Cancer*, **94**, 128–135.
- Wong, Y.H., Thomas, R.L., & Hawkins, G.F. 1978. Surface and subsurface structure of solids by laser photoacoustic spectroscopy. *Applied Physics Letters*, **32**, 538.
- Zhang, E.Z., Laufer, J.G., Pedley, R.B., & Beard, P.C. 2009a. In vivo high-resolution 3D photoacoustic imaging of superficial vascular anatomy. *Physics in medicine and biology*, **54**, 1035.
- Zhang, H.F., Maslov, K., Stoica, G., & Wang, L.V. 2006. Functional photoacoustic microscopy for high-resolution and noninvasive in vivo imaging. *Nature Biotechnology*, **24**, 848–851.
- Zhang, Q., Iwakuma, N., Sharma, P., Moudgil, B.M., Wu, C., McNeill, J., Jiang, H., & Grobmyer, H. 2009b. Gold nanoparticles as a contrast agent for in vivo tumor imaging with photoacoustic tomography. *Nanotechnology*, **20**, 395102.
- Zharov, V.P., Galanzha, E.I., Shashkov, E.V., Khlebtsov, N.G., & Tuchin, V.V. 2006. In vivo photoacoustic flow cytometry for monitoring of circulating single cancer cells and contrast agents. *Optics Letters*, **31**, 3623–3625.

VITA

Kiran was born in Hyderabad, Andhra Pradesh, India on September 3, 1988 and spent years 0-8 in India living in 3 different cities (Hyderabad, Durgapur, and New Delhi). After moving to the US in June 1997, his primary education was split up between California and Georgia. However, Kiran has lived in St. Louis and Columbia, Missouri for the largest portion of his life. He finished his undergraduate studies at the University of Missouri in 2011 with a degree in Biological Engineering.